DoE/ER/13749-3

SUMMARY

DOE/ER/13749--3

DE92 016085

PREVIOUS RESULTS

During the last two years we have continued our investigation of ultrasonic wave propagation in fluid-filled porous materials. First, we studied the feasibility of using different surface modes to characterize both synthetic and natural rocks. We introduced a novel experimental technique based on the direct generation of surface waves by edge excitation. We used two low-frequency (100-500 kHz) shear transducers in pitch-catch mode to launch and receive the ultrasonic surface wave. The contact transducers were coupled to the opposite edges of the porous specimens with normal polarization relative to the surface. The same technique was successfully used to generate Rayleigh-type surface modes on the free surface of both dry and water-saturated specimens, as well as Stoneley-type interface modes on the fluid-loaded surfaces of immersed samples. Our main achievement in this area is the realization that, due to surface tension, practically closed-pore boundary conditions can prevail on the free surface of a water-saturated rock for completely open pores. As a result, the velocity of the true surface mode might be much lower than the Rayleigh velocity of the dry skeleton. While the shear velocity drops a meager 2-5% upon saturating the specimen with water, the corresponding drop in the true surface wave velocity is a disproportional 20-50% for high-permeability rocks such as sandstones. This behavior is similar to the transformation of a Rayleigh-type surface mode to a much slower Stoneley-type true interface mode on the surface of a submerged solid while the original mode becomes leaky and quickly disappears. To the best of our knowledge, this is the first report on this kind of behavior of the *true surface wave on the free surface* of water-saturated rocks.

DISCLAIMER

Beside investigating guided acoustic waves in water-saturated porous materials, we also studied bulk wave propagation in air-saturated specimens. We further developed our experimental technique which is based on the transmission of airborne ultrasonic waves through air-filled porous plates. This method can be readily used to study the frequency-dependent propagation properties of slow compressional waves in different porous materials including natural rocks. By simple technical improvements, we extended the measuring range to 1-500 kHz, so that we could continuously cover *both low-frequency (diffuse) and high-frequency (propagating) regimes* of the slow wave propagation. In the diffuse region, which is usually below 100 kHz, both the velocity and the attenuation coefficient are primarily determined by the static permeability of the material. In the propagating region, the velocity depends on the tortuosity only while the attenuation coefficient depends also on the pore size and shape.

One of our main experimental results is that the *attenuation coefficient always approaches a linear dependence on frequency* at high frequencies. This means that the conditions for slow wave propagation do not improve at high frequencies in the way predicted by the Biot theory. The normalized attenuation coefficient, i.e., the total attenuation over one wavelength, is a key parameter in determining the feasibility of slow wave measurements by transmission-type experiments. In the diffuse region, the normalized attenuation coefficient is extremely high (≈60 dB). We found that in the propagating region it drops to a significantly lower value of 10 dB or so, but it also becomes constant. This unexpected behavior is due partly to increased viscous drag caused by surface roughness and inherent microscopic impurities and partly to elastic scattering caused by the uneven cross-section of the pore channels. These effects can be combined into a *new material parameter measuring the high-frequency dynamic permeability* of the material, which, together with the static permeability measured at lower frequencies in the diffuse

region, facilitates a more complete characterization of the pore structure. Experiments were made on well-defined metallic and ceramic porous materials as well as more complex real rocks of approximately 100 mD or higher permeability.

PROPOSED RESEARCH

During the next two years of this proposed work we plan to continue our investigation of ultrasonic wave propagation in fluid-saturated porous materials. This research effort should find applications in the geophysical evaluations of fluid-bearing porous rocks, where parameters such as tortuosity, shape factor, permeability, saturation level, and internal impurity are difficult to measure by conventional techniques using low-frequency acoustic or other methods. Our proposed work is focused on two novel experimental techniques developed during our current research project.

We have already demonstrated that, thanks to the surface tension effect, the true surface wave propagating on the free surface of a water-saturated rock can be readily used to assess the dynamic permeability of the specimen. We are going to further develop our direct excitation technique to increase the measuring accuracy by using special data acquisition techniques such as laser interferometric detection and more sophisticated signal evaluation methods including spectrum analysis and extensive spatial averaging. Our analytical efforts will be directed at developing an inversion method for evaluating the dynamic permeability from the velocity and attenuation coefficient of the true surface wave. In order to achieve this goal, further efforts will be made to study the frequency dependence of both propagation parameters. The suggested technique might well complement the currently used Stoneley wave technique whenever the surface is not submerged in the fluid, as in most borehole applications.

We are going to further develop our slow wave inspection technique for air-saturated porous solids, too. In particular, two basic problems of great practical importance will be addressed. First, we are going to modify our experimental arrangement so that both transmission and reflection of airborne ultrasonic waves can be used to evaluate the porous specimens. It is expected that, in this way, the permeability threshold, currently at approximately 100 mD, can be further reduced by at least one order of magnitude. Such improvement would extend the field of application of this simple material characterization technique to many oil-bearing rocks of practical importance. Second, we are going to study the effect of partial water-saturation on the low- and high-frequency behavior of the dynamic permeability. These results might find important applications in developing new experimental techniques to measure the relative permeability in porous materials.

I. PROGRESS REPORT

Ultrasonic evaluation of porous materials can take advantage of some very specific acoustic phenomena which occur only in fluid-saturated consolidated solids of continuously connected pore structure. Certain material properties of the porous frame such as the degree of consolidation or grain size can be readily evaluated from the velocity or attenuation of the shear and longitudinal waves in the dry skeleton or those of the fast compressional wave in the fluid-saturated material.[1,2] Other parameters such as tortuosity, permeability, porosity, and pore size, shape and surface quality are inherently connected to the porous nature of the material and can be evaluated much better from the propagation properties of the slow compressional wave. Unfortunately, the slow compressional wave is usually very weak due to high attenuation caused by viscous drag between the fluid and the solid frame. In natural rocks, the viscous drag is further increased by clay particles deposited both within the pore throats and on the surfaces of the rock grains.[3] The excessive attenuation results in the complete disappearance of the slow compressional mode in water-saturated rocks. Because of this, we have to introduce two novel experimental approaches which are more suitable to geophysical applications where the economic benefits of ultrasonic material characterization are enormous.

First, we studied the feasibility of using different surface modes to characterize the properties of water-saturated rocks. This technique is based on the indirect observation of the slow compressional wave through its significant effect on the velocity of the surface mode propagating along the free surface of the wet rock. Second, we also studied bulk slow wave propagation in air-filled porous materials. Due to the relatively high kinematic viscosity of air, the slow compressional wave is even more attenuated than in water-saturated samples, but it is the only mode which is generated with a significant amplitude, therefore

its detection is fairly simple. The main results of these two research efforts are discussed separately in the following chapters.

1.1 SURFACE WAVE TECHNIQUE

As we have mentioned before, the bulk slow wave propagating in a water-saturated natural rock is usually far too weak to be detected, let alone to be used for material characterization. On the other hand, surface and interface waves guided along the contour of a water-saturated specimen are much less attenuated but still quite sensitive to the permeable nature of the porous formation. Maybe the best example is a borehole Stoneley wave which is the fundamental mode of a guided wave traveling in a fluid-filled tube. In the case of permeable walls, because of fluid flow into the formation, the Stoneley wave velocity decreases and its attenuation increases. The strong correlation between the frequency-dependent propagation parameters and formation permeability can be exploited in acoustic logging in the field or in the laboratory.[4-8] It has been suggested that other types of guided modes can be used in a similar way to assess formation permeability, tortuosity, and other parameters of a porous material.[9-11]

1.1.1 INTRODUCTION AND BACKGROUND

There is only one type of true interface wave which can propagate along the free surface of an ordinary solid. It is called Rayleigh wave and its velocity is approximately 5-10% below the shear wave velocity. Two types of interface waves can propagate along the fluid-loaded surface of an immersed ordinary solid: there is a true mode called Stoneley (or sometimes Scholte) wave and a pseudo-mode called leaky Rayleigh wave. The true wave is always slower than all the bulk waves in the solid

and the fluid and it produces evanescent fields only as it propagates along the interface. Since the energy of this mode is strictly confined to the interface region, its generation and detection presents a rather difficult technical problem. The leaky Rayleigh wave is slightly faster than the true Rayleigh wave propagating on the free surface of a solid. In most cases, this velocity is faster than the sound velocity in the fluid, therefore it leaks energy into the liquid as it propagates along the interface. This mode can be easily generated and detected by the phase-matching compressional wave in the fluid at the so-called Rayleigh angle, at least whenever this angle is not much higher than 60°. It should be mentioned that this mode becomes non-propagating whenever the shear velocity in the solid is lower than the sound velocity in the fluid, which is true for many natural rocks.

Of course, the situation becomes much more complex in the case of a fluid-saturated porous solid. Feng and Johnson showed that a maximum of three different types of surface modes can exist on a fluid/fluid-saturated porous solid interface depending on (i) the shear velocity of the frame and (ii) the surface conditions, i.e. whether the pores are open or closed.[9,10] However, in most natural rocks the shear velocity is lower than the sound velocity in water and the pores are open at the surface, therefore there is but one principal surface mode, namely the Stoneley mode. It is important to realize that this mode becomes leaky into the slow compressional wave whenever its velocity is higher, as it is in most cases of interest to us. Although the slow wave is very highly attenuated and cannot be directly observed in water-saturated rocks, its indirect effect of making the Stoneley wave highly attenuated via this leakage can be more readily observed. This attenuation mechanism is taken advantage of for permeability assessment in the Stoneley borehole technique. Of course, in the case of an impermeable ordinary solid, the Stoneley wave is a true interface wave with lower velocity than any of the bulk velocities in the surrounding

media.

To the best of our knowledge, the corresponding effect on the true surface wave propagating on the free surface has not been investigated yet in the open literature. Although the surface is free, the Rayleigh wave must become leaky into the slow compressional mode unless its velocity is lower. On the other hand, for well consolidated rocks of relatively high frame modulus, the shear velocity is similar to the compressional wave velocity in water. Since the Rayleigh velocity is approximately 90-95% of the shear velocity while the slow wave velocity is only 50-70% of the sound velocity in water, it is expected that the Rayleigh mode becomes leaky in most water-saturated natural rocks. At the same time, the true surface wave, if there is one, must propagate with a velocity lower than the slow wave velocity so that it cannot leak energy into the bulk of the material. In the next chapter we present our new analytical results for the velocity and attenuation coefficient of the modified Rayleigh wave propagating on the free surface of a water-saturated permeable solid. In the subsequent two chapters we describe our experimental technique and results and present a short discussion of these results showing the feasibility of the suggested surface wave technique for measuring formation permeability of water-saturated rocks.

1.1.2 ANALYTICAL RESULTS

The method of Feng and Johnson[9,10] can be easily applied to the case of a surface wave propagating along the free surface of a water-saturated rock. It is even easier and also more realistic, to assume that the superstrate fluid is air while the substrate is saturated with water. Of course, the sound velocity in air is only 340 m/s, therefore the surface wave is always leaky into the superstrate. On the other hand, due to the very low density of air, this leakage is quite negligible and the

surface can be considered "free" for all practical purposes.

We are going to show that capillary forces can hold the wetting fluid (water) in the pores and effectively extend a membrane over the surface pores at the boundary with the non-wetting fluid (air). This membrane is usually so strong that it assures closed-pore boundary conditions at the surface. Of course, the same formation exhibits open-pore boundary conditions at the water/water-saturated porous solid interface when the specimen is fully immersed in water.

In the ideal case of completely closed surface pores and viscosity-free fluid, two types of surface wave can propagate along the free surface of a fluid-saturated porous solid. First, there is a pseudo-Rayleigh mode which leaks its energy into the slow compressional wave. In the case of a highly permeable solid, the resulting attenuation might be quite significant. Second, there is a true surface mode with velocity slightly below that of the slow wave. This mode is a simple form of realization of the new interface mode predicted by Feng and Johnson[9,10] when the superstrate fluid is extremely rare and highly compressible like air.

First, we will show through the example of the true surface mode that a minimum surface stiffness of approximately $10^{10}N/m^3$ is required to produce close-pore boundary conditions. Second, we will demonstrate that strong capillary forces in water saturated natural rocks can easily produce a surface stiffness in excess of $10^{10}N/m^3$, therefore the pores are effectively closed at the surface of a water-saturated rock surrounded by air. Third, we will show that under these conditions, the surface velocity is very sensitive to the dynamic permeability of the porous sample.

Table 1 shows the material parameters used in the following calculations. A detailed description of the boundary conditions and the derivation of the characteristic equation can be found in

Reference 9. The surface stiffness T_s is defined as the proportionality coefficient between the discontinuity in pressure and relative displacement of the fluid with respect to the frame below the interface:

$$p-p' = T_s\phi(U_z-u_z), \tag{1.1}$$

where p and p' denote the fluid pressure in the pore space below the surface and in the superstrate fluid just above it, respectively. U_z and u_z are the normal displacement components of the fluid and solid below the surface, and ϕ denotes the porosity. We adapted this form for the boundary condition because it suits our immediate purposes better than the more general solution of defining a surface impedance Z_s by[4,12]

$$p-p' = i\omega Z_s\phi(U_z-u_z), \tag{1.2}$$

where ω denotes the angular frequency. In the case considered here, the finite surface impedance is due to an apparent membrane extended over the surface pores by capillary forces and its stiffness depends on the surface tension of the fluid. In the case of a fluid/fluid-saturated porous solid interface (e.g., in borehole Stoneley wave experiments), the finite surface impedance is due to the flow resistivity of the surface pores and its value depends on the viscosity of the fluid. Naturally, in this case the definition of Equation 1.2 is easier to adapt. Otherwise, there is no physical difference between the two approaches and the surface impedance can be expressed by the surface tension as

$$Z_s = T_s/i\omega. \tag{1.3}$$

Table 1 Material parameters used in the surface wave calculations.

superstrate (air) density	1.3	10^0	kg/m^3
superstrate (air) bulk modulus	1.5	10^5	N/m^2
substrate fluid (water) density	1.0	10^3	kg/m^3
substrate fluid (water) bulk modulus	2.25	10^9	N/m^2
substrate solid (glass) density	2.48	10^3	kg/m^3
substrate solid (glass) bulk modulus	4.99	10^{10}	N/m^2
frame bulk modulus	6.64	10^9	N/m^2
frame shear modulus	3.69	10^9	N/m^2
porosity	0.3		
tortuosity	1.79		

Feng and Johnson considered two special limiting cases only: (i) $T_s=0$ (i.e., $p=p'$) corresponds to an open-pore situation with free flow of fluid in and out of pores and (ii) $T_s=\infty$ (i.e., $U_z=u_z$) corresponds to a closed-pore situation at the surface when there is no relative flow. We extended these calculations to the more general case of finite surface stiffness. Table 2 lists the different bulk and surface wave velocities in dry (air-saturated) and wet (water-saturated) porous glass. A number of important features should be noticed here. The fast compressional wave velocity is approximately 12% higher while the shear velocity is 4% lower in the wet sample. The small drop in the shear velocity is particularly important since (i) it provides a direct measure of the inertia effect of the fluid moving within the porous solid and (ii) the shear wave velocity is very closely related to the Rayleigh velocity on the free surface. In the high frequency limit, when viscous drag between the fluid and the frame is negligible, the shear wave velocity v_s can be expressed by

$$v_s^2 = N/[(1-\phi)\rho_s+\phi\rho_f(1-1/\tau)], \qquad (2)$$

Table 2 Sound velocities in dry and wet porous glass.

	dry	wet
fast wave	2,580 m/s	2,879 m/s
slow wave	254 m/s	980 m/s
shear wave	1,458 m/s	1,405 m/s
surface wave		
- open pores	1,344 m/s	1,295 m/s
- closed pores	1,344 m/s	880 m/s

where N is the shear modulus of the dry frame, ρ_s and ρ_f denote the solid and fluid densities, respectively, and τ is the tortuosity. As opposed to the compressibility of the material, the rigidity is not affected by fluid saturation, therefore the relative difference between the shear velocities of the dry and wet samples depends mainly on the tortuosity:

$$(v_s^{(dry)} - v_s^{(wet)})/v_s^{(dry)} \approx 1/2\ \rho_f/\rho_s\ \phi/(1-\phi)\ (1-1/\tau), \quad (3)$$

where the densities and the porosity can easily be determined from simple weight measurements. Theoretically, Equation 3 can be readily exploited to determine the tortuosity by comparing the shear velocities in the dry and wet samples. Unfortunately, the sensitivity to the tortuosity is rather low. For example, the relative change in the shear velocity increases from 5.7% to 6.5% as the tortuosity increases from 3 to 4. Although we could easily measure the shear wave velocity with a relative accuracy of 0.1%, the inertia effect might be overshadowed by inevitable small changes in the rigidity of the sample as we saturate the solid. From this point of view, a water-saturated natural rock might behave significantly differently from an ideal Biot-solid. This discrepancy can be caused by a variety of different mechanisms such as dehydration and stiffening of clay minerals, ionization, adsorbed water, capillary forces, etc.[13] In conclusion, the small

change in shear velocity cannot be used reliably to assess the tortuosity, but the change is usually negative and only a few percent.

Going back to Table 2, we can also note that, for a dry sample, the surface wave velocity is approximately 7.8% lower than the shear velocity, regardless whether the surface pores are open or closed. There is only negligible coupling between the solid frame and the air and the sample behaves like an ordinary solid. For open pores, water saturation gives very similar results as the surface velocity is again approximately 7.8% lower than the shear velocity (of course, both velocities are somewhat lower in the wet sample due to the above mentioned inertia effect, but their ratio is the same). On the other hand for closed pores, the velocity of the true surface wave becomes much (approximately 30%) slower than the shear velocity. Actually, it is even slower than the slow compressional wave at 980 m/s. This has to be so since it is a true surface wave and due to the closed pores at the surface it would otherwise leak energy into the slow compressional wave. In the case of open pores at the surface, a disturbance can propagate along the surface without generating a slow wave component since, in the absence of viscosity, there is nothing to prevent the water from flowing through the surface pores without producing a reaction force. On the other hand, when the surface pores are closed, the surface mode becomes very similar to the slow compressional wave itself although its velocity is slightly lower. This small difference further diminishes as the frame modulus increases. In the case of a very rigid frame with closed pores at the surface the slow compressional wave alone satisfies the free boundary conditions (like a horizontally polarized shear wave does in an ordinary solid).

Figure 1 and 2 show the calculated velocity and attenuation coefficient of the "true" surface wave propagating on the surface of a water-saturated porous material as a function of the surface

stiffness. The dependence of the propagation parameters on the surface stiffness is very similar to the frequency dependence caused by a single relaxation process. The velocity drops from 1,295 m/c to 880 m/s as the surface stiffness increases. There is a fairly sharp turning point around $10^7 N/m^3$ where the attenuation exhibits a maximum. The attenuation coefficient is calculated from the imaginary part of the complex root of the characteristic equation. Since the characteristic equation is independent of frequency, the solution is non-dispersive and the attenuation coefficient turns out to be linearly proportional to frequency. Let $v=v_r+iv_i$ denote the complex root of the characteristic equation. Then

$$\exp[i\omega(t-x/v)] = \exp[i\omega(t-x/v_p)] \exp[-\alpha x], \qquad (4.1)$$

where v_p denotes the phase velocity

$$v_p = (v_r^2+v_i^2)/v_r, \qquad (4.2)$$

and α is the attenuation coefficient

$$\alpha = \omega v_i/(v_r^2+v_i^2). \qquad (4.3)$$

In order to retain the generality of the relationship between the attenuation coefficient and the surface stiffness, we plotted the attenuation slope, i.e., attenuation coefficient divided by frequency, in Figure 2. The maximum at approximately 10^7 N/m^3 corresponds to a rather high 7 dB/cm attenuation coefficient at 100 kHz. Since the wavelength is close to 1 cm, the normalized attenuation coefficient, i.e., the attenuation over one wavelength, is 7 dB. This corresponds to a very strongly attenuated but still propagating wave within the reach of experimental observation. Of course, at both lower and higher surface stiffness, the surface wave becomes much less attenuated. In the case of finite surface stiffnesses, the surface wave is coupled to the slow compressional wave of lower velocity

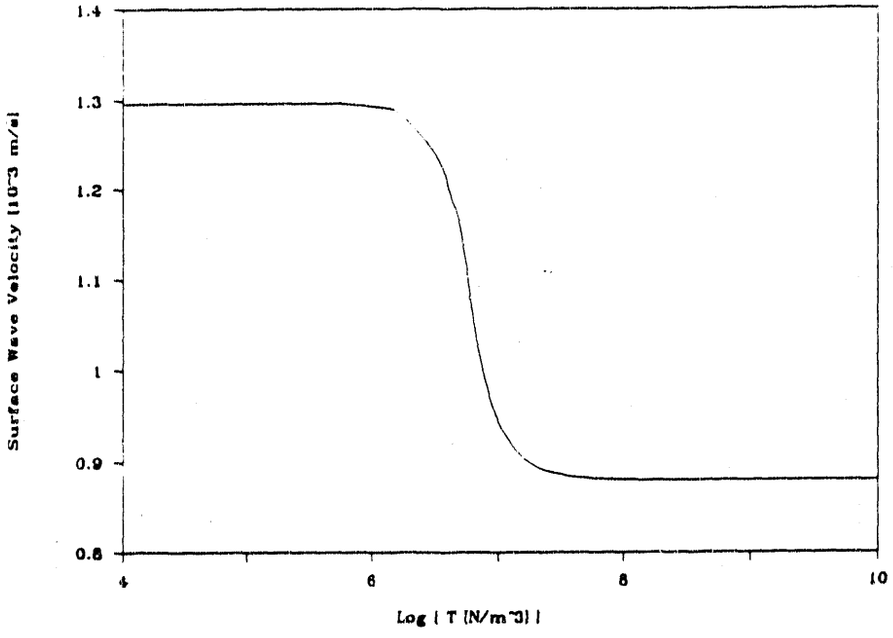

Figure 1 Surface wave velocity versus surface stiffness on the free surface of a wet rock.

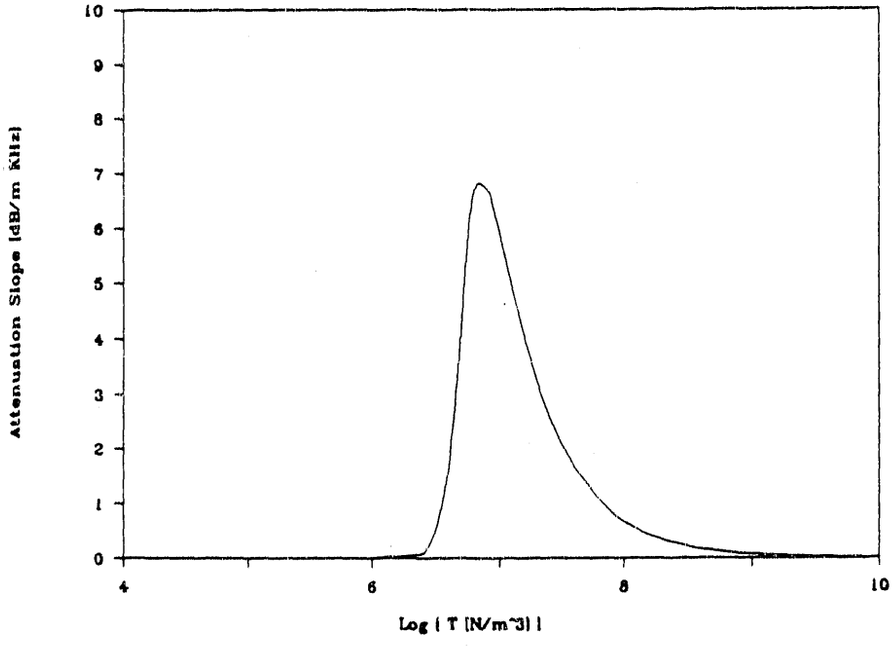

Figure 2 Surface wave attenuation versus surface stiffness on the free surface of a wet rock.

therefore it is attenuated by leakage of energy into that mode.

If we were to assess the velocity and attenuation coefficient of a Stoneley-type interface wave along a fluid/fluid-saturated porous solid boundary, we would have to calculate the surface resistivity from the formation permeability and the fluid viscosity. Similarly, in order to assess the propagational parameters of the Rayleigh-type surface wave along the free surface of a fluid-saturated porous solid, we have to calculate the surface stiffness from the formation permeability and the surface tension of the fluid. For the sake of simplicity, let us assume that the pores are cylindrical holes of radius a. The radius of the surface membrane can be calculated from the Laplace equation:

$$R = 2\sigma/p_f, \tag{5}$$

where σ denotes the surface tension and p_f is the fluid pressure:

$$p_f = p_o - p, \tag{6}$$

where p_o and p denote the hydrostatic and acoustic pressure, respectively. Capillary forces can pull the fluid column to a maximum height h where the hydrostatic pressure reduces the radius of the surface membrane to that of the pore, a:

$$h = 2\sigma/\rho_f g a, \tag{7}$$

where g is the gravitational acceleration. In natural rocks, the capillary height can be as large as a few meters and, of course, the hydrostatic pressure is much larger than the acoustic component. The fluid volume in the pore can be written as

$$V_f = V_p - a^4\pi/4R, \tag{8}$$

where V_p denotes the total volume of the pore. A small change of

the membrane's radius dR causes

$$dV_f = dR\ a^4\pi/4R^2 \tag{9}$$

change in the fluid volume. From Equations 5 and 6,

$$dR = pR^2/2\sigma \tag{10}$$

and the surface stiffness can be obtained by substituting Equation 10 into Equation 9 and then into Equation 1 and using the simple relationship between the average fluid displacement and the volume velocity

$$(U_z - u_z)\ a^2\pi = dV_f. \tag{11}$$

Finally,

$$T_s = 8\sigma/\phi a^2. \tag{12}$$

For a network of cylindrical pores, the combination of the Darcy and Poiseuille laws give the following well-known equation for the static permeability

$$\kappa_o = \phi a^2/8, \tag{13}$$

which can be used to establish a simple relationship between the surface stiffness and the formation permeability:

$$T_s = \sigma/\kappa_o. \tag{14}$$

For water, σ=2.3 10^{-2}N/m, and even a relatively high static permeability of κ_o=1,000 mD $\approx 10^{-12}$ m^2 produces a surface stiffness in excess of 10^{10} N/m^3. A quick comparison with Figures 1 and 2 verifies that, for all practical purposes, the pores are sealed by such surface tension on the free surface of a water-saturated rock. Since the true surface mode effectively becomes a

weakly perturbed slow wave, its attenuation is expected to be as high as that of the slow wave. This phenomenon is analogous to the relation between the Rayleigh-type true surface mode propagating on the free surface of an ordinary solid and the shear wave or that of the Stoneley-type true interface wave propagating along a fluid/ordinary solid boundary and the compressional wave in the fluid. Whenever the slow compressional wave is killed by excessive attenuation, the true surface mode is expected to suffer a similar fate. Therefore, in natural rocks of low permeability (less than 100 mD) the dominant surface mode is expected to switch over to the leaky Rayleigh mode.

Up to this point, viscous losses were completely neglected. Actually, they play a very important role in both attenuation and velocity of the surface wave. The easiest way to model viscous losses in the fluid-saturated porous solid is to assume a complex tortuosity rather than a pure real one based simply on the geometry of the pore channels. The complex tortuosity $\tau(\omega)$ is related to the dynamic permeability $\kappa(\omega)$ of the specimen:[14]

$$\tau(\omega) = i\eta\phi/\omega\kappa(\omega), \tag{15.1}$$

where η is the kinematic viscosity of the saturating fluid, and the complex wave number k can be expressed as

$$k(\omega) = \omega\tau^{1/2}(\omega)/v_f. \tag{15.2}$$

It has been shown that the complex tortuosity has a nearly universal form determined by four basic parameters, namely the high-frequency tortuosity τ_∞, the static permeability κ_o, the porosity ϕ, and a length parameter Λ determined by the average pore size and shape:[14]

$$\tau(\omega) = \tau_\infty + i(\eta\phi/\omega\kappa_o)(1-4i\tau_\infty^2\kappa_o^2\omega/\eta\Lambda^2\phi^2)^{1/2}. \tag{16.1}$$

Relatively small viscous effects can be accounted for by a

simplified version of this general form:

$$\tau(\omega) \approx \tau_\infty[1+(iL)^{1/2}], \tag{16.2}$$

where L denotes the loss factor

$$L = 4\eta/\omega\Lambda^2. \tag{16.3}$$

Figures 3 and 4 show the calculated velocity and attenuation coefficient of the "true" and leaky Rayleigh surface waves propagating on the free surface of a water-saturated porous solid in the case of closed-pore boundary conditions. The velocity of the "true" surface mode increases significantly with increasing viscous losses. The attenuation slope (attenuation coefficient divided by frequency) also increases at first, then flattens off as the loss factor reaches approximately 10%. The leaky Rayleigh velocity is much less affected by the complex nature of the tortuosity. Its velocity drops slightly as the fluid becomes immobilized within the pores. This small drop in velocity is primarily due to the added inertia effect of the fluid, which affects the shear wave in a similar way (see Equations 2 and 3). Its attenuation slope is basically constant since the loss is mainly due to energy leakage into the slow compressional wave. This loss is more or less the same whether the slow wave is strongly attenuated or not. Experimental results indicate that in real water-saturated rocks the shear wave is much more attenuated than is predicted by the Biot theory. Similarly, we expect that the Rayleigh-type surface wave is also much more attenuated than one would assume from these simple calculations.

The most important conclusion we can draw from these results is that not only the attenuation, but also the velocity of the "true" surface wave is greatly affected by the loss factor, i.e., the dynamic permeability of the porous solid. According to our calculations, in low-permeability rocks, the surface wave velocity drops but a meager 3-4% when the sample is saturated by

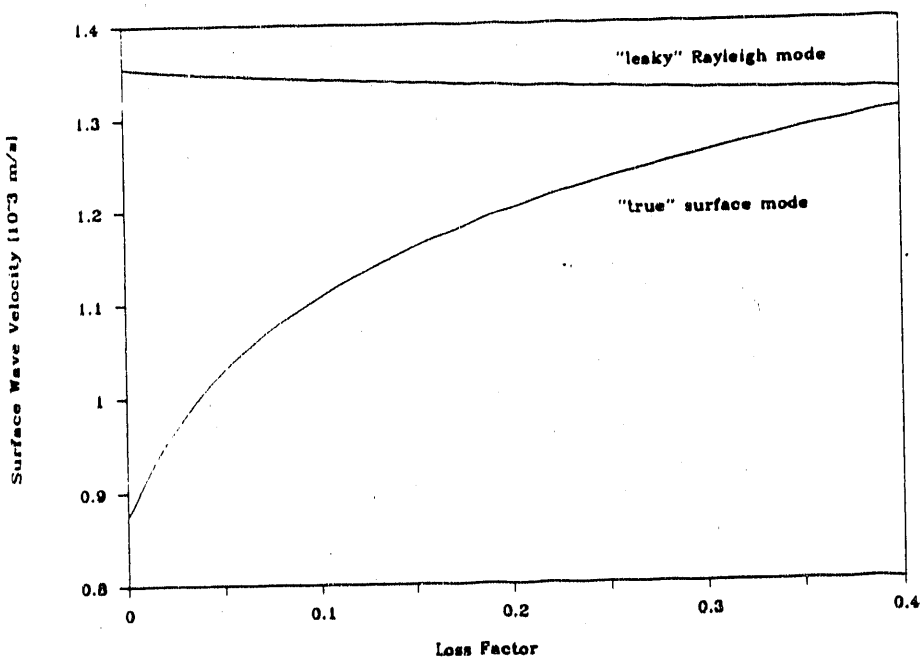

Figure 3 Surface wave velocity versus loss factor on the free surface of a wet rock.

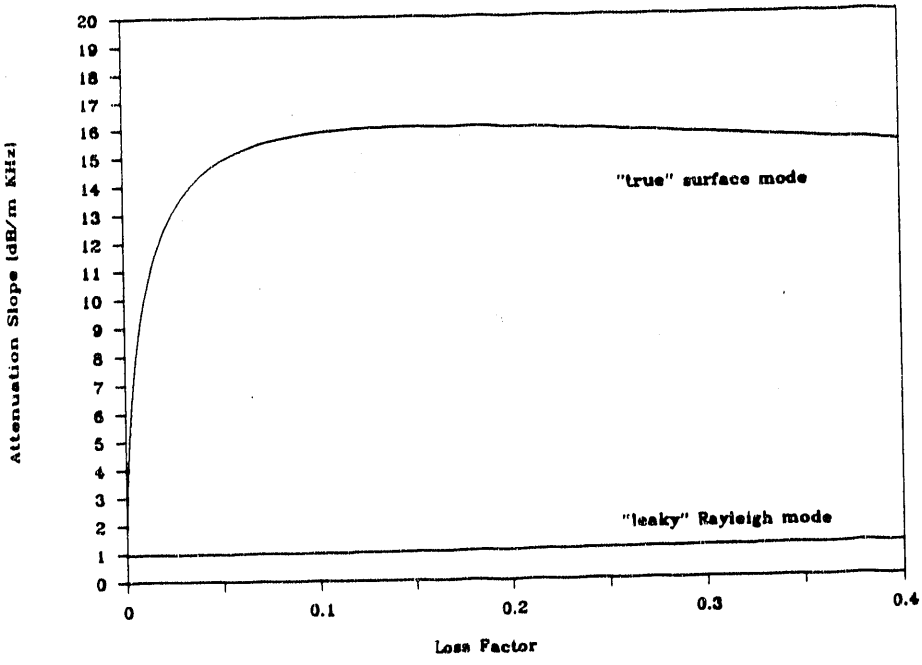

Figure 4 Surface wave attenuation versus loss factor on the free surface of a wet rock.

water. On the other hand, in high-permeability samples, the corresponding drop might be as much as 30-40%, i.e., one order of magnitude larger. Our experimental efforts were focused on verifying these predictions.

1.1.3 EXPERIMENTAL TECHNIQUE AND RESULTS

Recently, we have introduced a new experimental technique for surface and interface wave generation by direct excitation using conventional contact transducers.[15,16] The schematic diagram of the experimental arrangement is shown in Figure 5. Two contact transducers are placed directly over the opposite edges of the specimen so that they can generate a bulk mode in the interior of the sample as well as guided modes along the surface. In this particular case, we used shear transducers of vertical polarization, i.e., normal to the surface. Figure 6 shows the detected signals on a 90-mm-long aluminum sample. The first arrival is a shear-type bulk wave which is followed by a slightly slower Rayleigh-type surface wave. It is important to notice that the bulk signal is much sharper, i.e., it has more high-frequency components than the surface mode. This difference raises the question of energy partition between the two principal modes of propagation. The center part of the transducer, which is directly over the interface region within approximately one wavelength, generates mostly surface modes while the lower part, which is father away from the surface, generates mostly bulk waves. According to this very simple model, the total energy will be divided between the surface and bulk modes proportionally to the ratio between the wavelength and the transducer radius. Since the wavelength is inversely proportional to frequency, the low-frequency components contribute to the surface mode only while the high-frequency components go mostly into the bulk mode. This conclusion is confirmed by Figure 7 showing the complemental

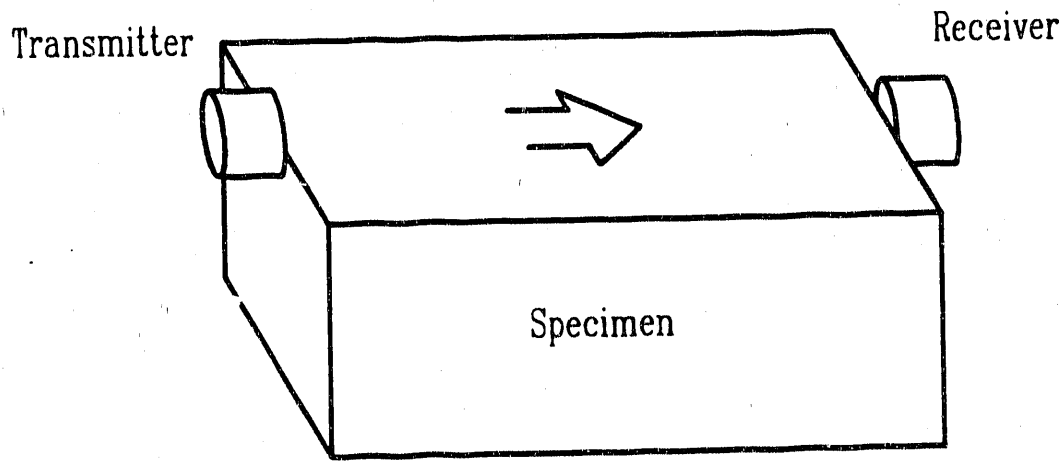

Figure 5 Geometrical arrangement for direct surface wave generation.

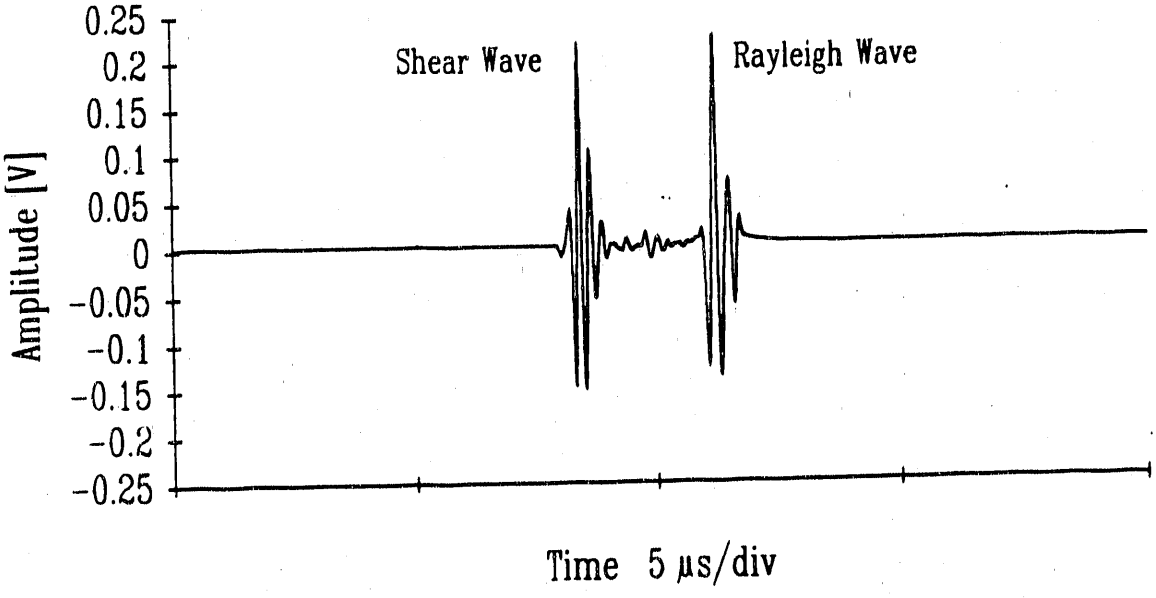

Figure 6 The received signals through a 90-mm-long aluminum sample.

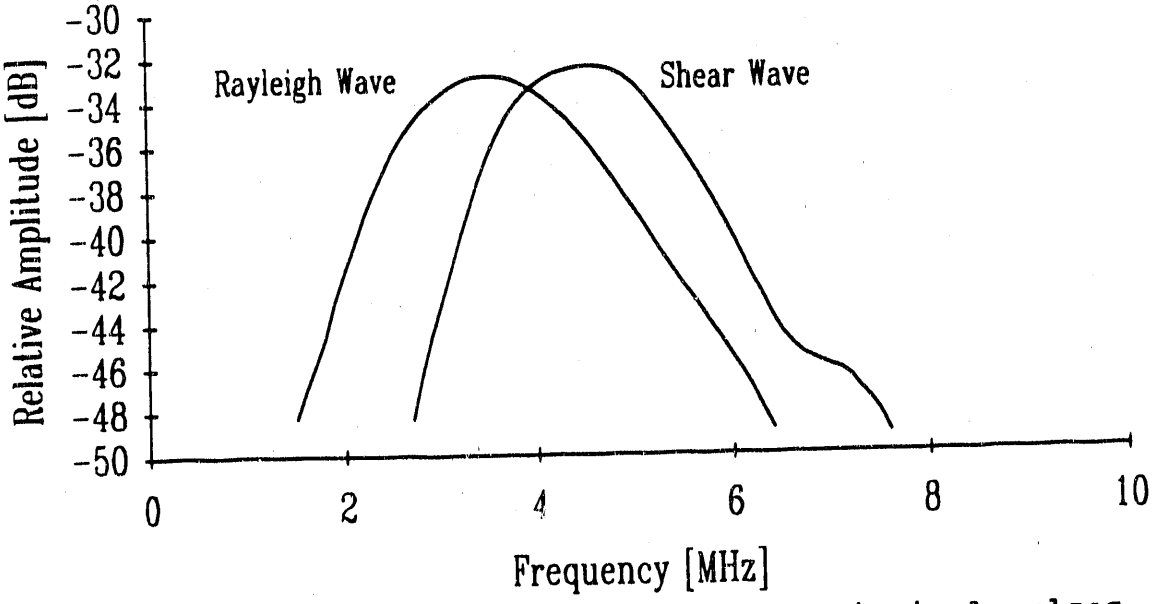

Figure 7 Frequency spectra of the two principal pulses shown in Figure 6.

frequency spectra of the two principal pulses of Figure 6. Since the high-frequency components are usually much more attenuated in both dry and wet porous materials than in aluminum, the surface mode becomes the stronger of the two.

As opposed to bulk modes, surface modes are not polarized strictly normal or parallel to the propagation direction. Therefore, the vertically polarized shear transducer might be replaced by a longitudinal transducer. In the case of true or leaky Rayleigh waves, the polarization is dominantly normal to the surface therefore a shear transducer gives somewhat better sensitivity. In the case of a Stoneley-type interface wave propagating along a fluid/high-density solid boundary, the polarization is dominantly parallel to the interface and a longitudinal transducer should be used. In the case of a low-density solid, like most natural rocks, the Stoneley-type interface wave is strongly coupled to both media and the particle displacement has significant components in both directions therefore either shear or longitudinal transducers would work. Actually, in the case of a longitudinal transducer, the operation is rather similar to the widely-used borehole Stoneley wave technique, although the axisymmetric arrangement is obviously more sensitive.

Previously, we successfully used this technique to generate and detect Stoneley-type interface modes propagating along fluid/fluid-saturated porous solid interfaces. This time, we concentrated on the apparently simpler case of Rayleigh-type surface modes propagating on the free surface of both dry and wet porous solids. Because of the excessive attenuation of the high-frequency components in real rocks, the shear wave is usually too weak to be detected in the presence of the much stronger low-frequency surface wave. Therefore, we measured the shear wave velocity by simply moving the transducers from the surface to the interior of the sample where the shear wave produced the only detectable signal.

Figure 8 shows the significant change in the time of arrival of the shear component upon saturating a Sunset Blush Massillon Sandstone sample with water. The detected signal was digitally recorded at 5-second-intervals. The sample's thickness was 52 mm and the shear velocity was found to be approximately 1,620 m/s in the dry sample. In order to clearly demonstrate the effect of water-saturation on the velocity of the transmitted shear wave, we kept the signal amplitude at its initial level by continuously increasing the gain of the receiver. Actually, the signal amplitude dropped by 23 dB during the experiment, which explains the somewhat higher noise level observed after approximately three minutes saturation time. It is less apparent that the shape of the signal has changed a little, too, as the high-frequency components are much more attenuated than the low-frequency ones.

Figure 9 shows the additional attenuation caused by water-saturation. The experimental data was obtained by subtracting the modulus of the frequency spectrum of the first signal in Figure 8 (completely dry rock) from that of the last one (completely wet rock). The solid line is the best fitting linear regression. The induced attenuation seems to be proportional to frequency and the above mentioned 23 dB gain adjustment needed to keep the peak-to-peak amplitude constant during the experiment is approximately the same as the actual attenuation at 160 kHz, i.e., at the center of the frequency band. The induced time delay is approximately 2 μs corresponding to 5.6% drop in the shear wave velocity. This change is in reasonably good agreement with our expectations based on the added inertia effect. By assuming $\rho_s/\rho_f=2.3$, $\phi=23\%$ connected porosity, and $\tau=3$ tortuosity, Equation 3 gives 4.3%. As we have mentioned before, better quantitative agreement cannot be expected because of the simplicity of the model used to derive the shear wave velocity in a fluid-saturated porous rock.

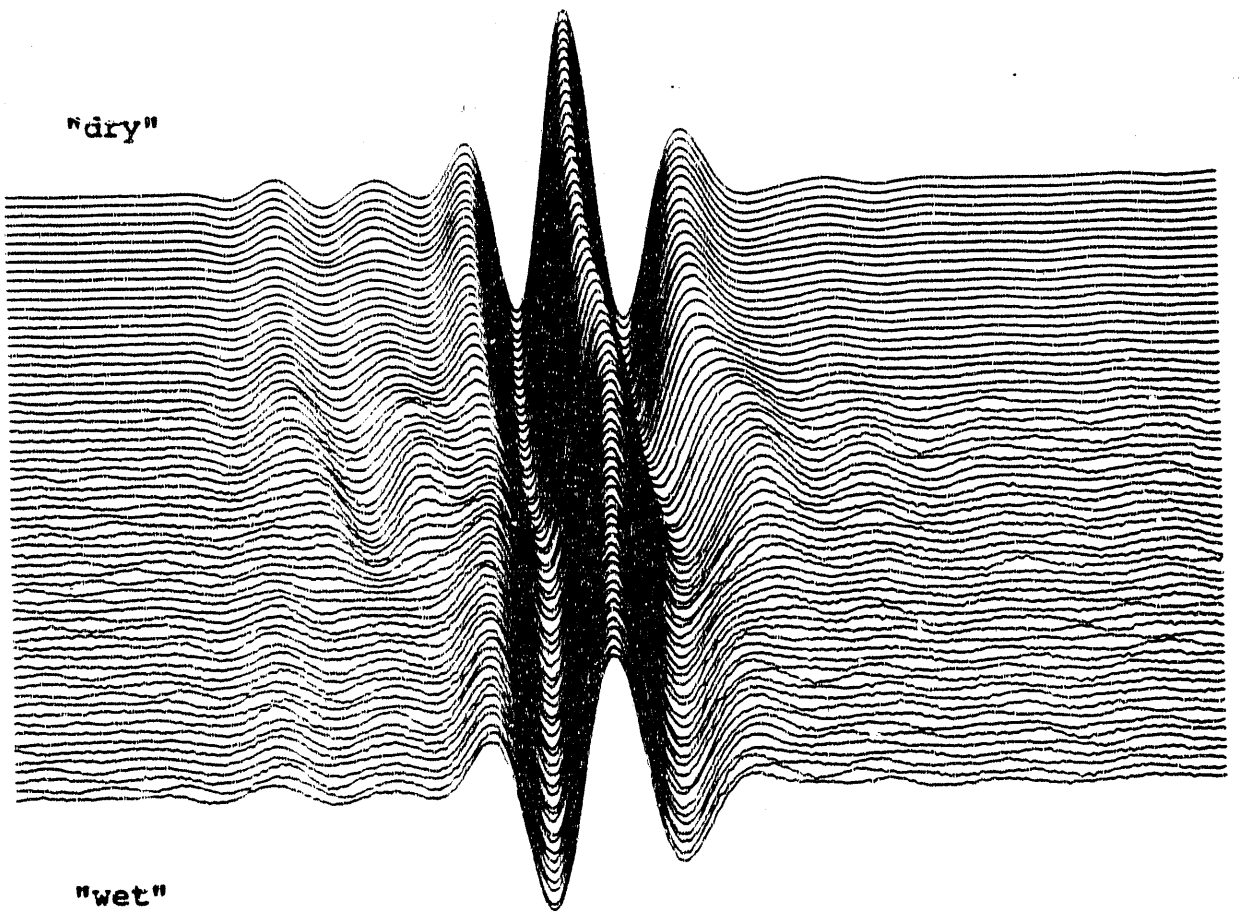

Figure 8 The effect of gradual water-saturation on the transmitted shear wave through a 52-mm-thick Sunset Blush Massillon Sandstone specimen. Vertical scale (saturation time) is 6 minutes, horizontal scale (propagation time) is 60 μs.

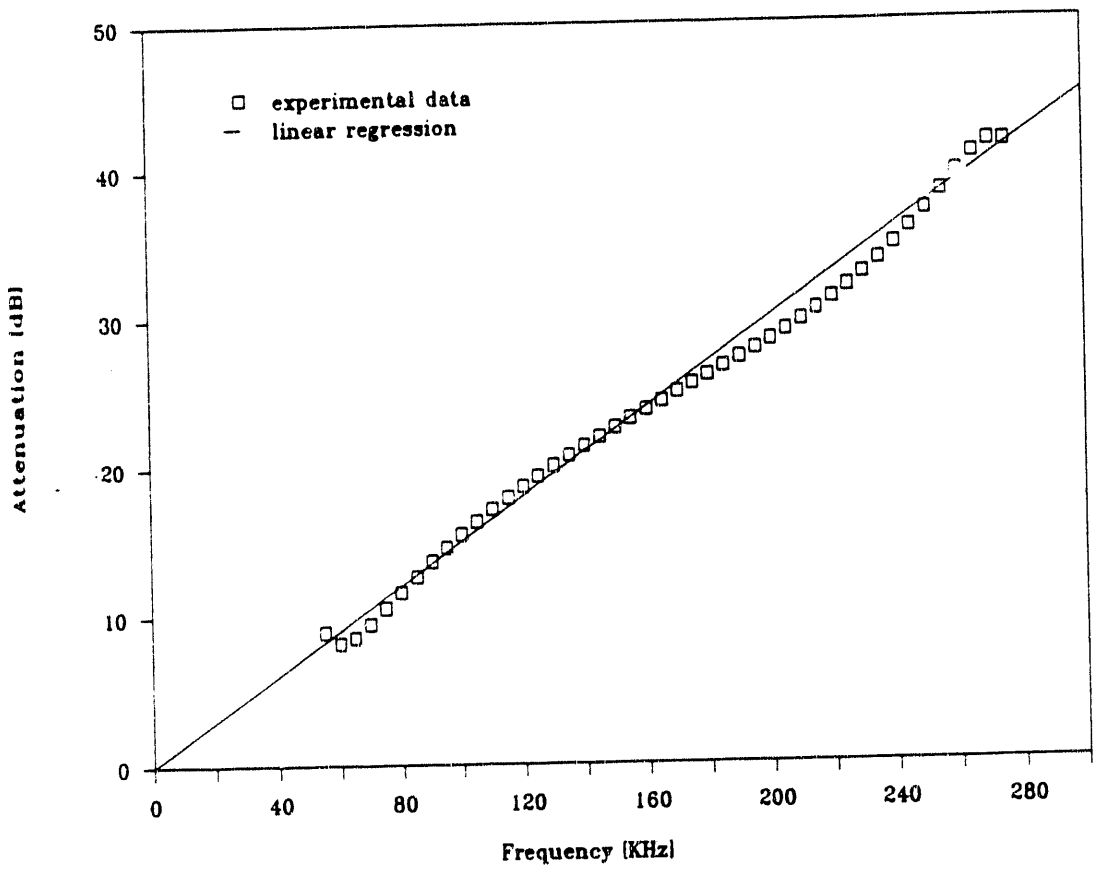

Figure 9 Saturation induced attenuation of the shear wave in a 52-mm-thick Sunset Blush Massillon Sandstone specimen as a function of frequency.

In order to establish the feasibility of the suggested experimental technique for surface wave velocity measurements in natural rocks, we have measured the velocity of the dominant surface mode in a number of both dry and wet rocks. The 1"-diameter, low-frequency (100-500 kHz) shear transducers were pressed against the samples by a constant weight of approximately 30 lbs. All samples were cut into rectangular blocks so that two significantly different dimensions were accessible for comparison. The "short" and "long" dimensions were typically 2 and 4 inches, respectively. As an example, Figure 10 shows the detected surface wave signals on a Cavallo Buff Massillon Sandstone specimen in dry and wet conditions. The surface wave velocity was directly calculated from the differences in propagation length and time. Table 3 summarizes our experimental results on 16 different rocks used in this study. The experimental uncertainty is estimated to be approximately 5%. The main source of this significant experimental error is the distortion of the shape of the observed signals which renders the overlapping, and therefore the time delay measurement, too, somewhat uncertain. Also, because of the inherent inhomogeneity and anisotropy of most natural rocks, the accuracy of such measurements is inherently limited.

On the average, the Rayleigh velocity in the dry samples (1,610 m/s) is 10% lower than the shear velocity (1,790 m/s), while the surface wave velocity in the water-saturated samples (1,400 m/s) is 13% lower than in the dry ones. The ratio between the experimentally determined surface wave velocities is clearly higher than the approximately 5% one would expect from the inertia effect of water-saturation. The uneven distribution of this ratio is even more interesting: it is in excess of 30% in the five most permeable rocks but only a few percent for the least permeable ones.

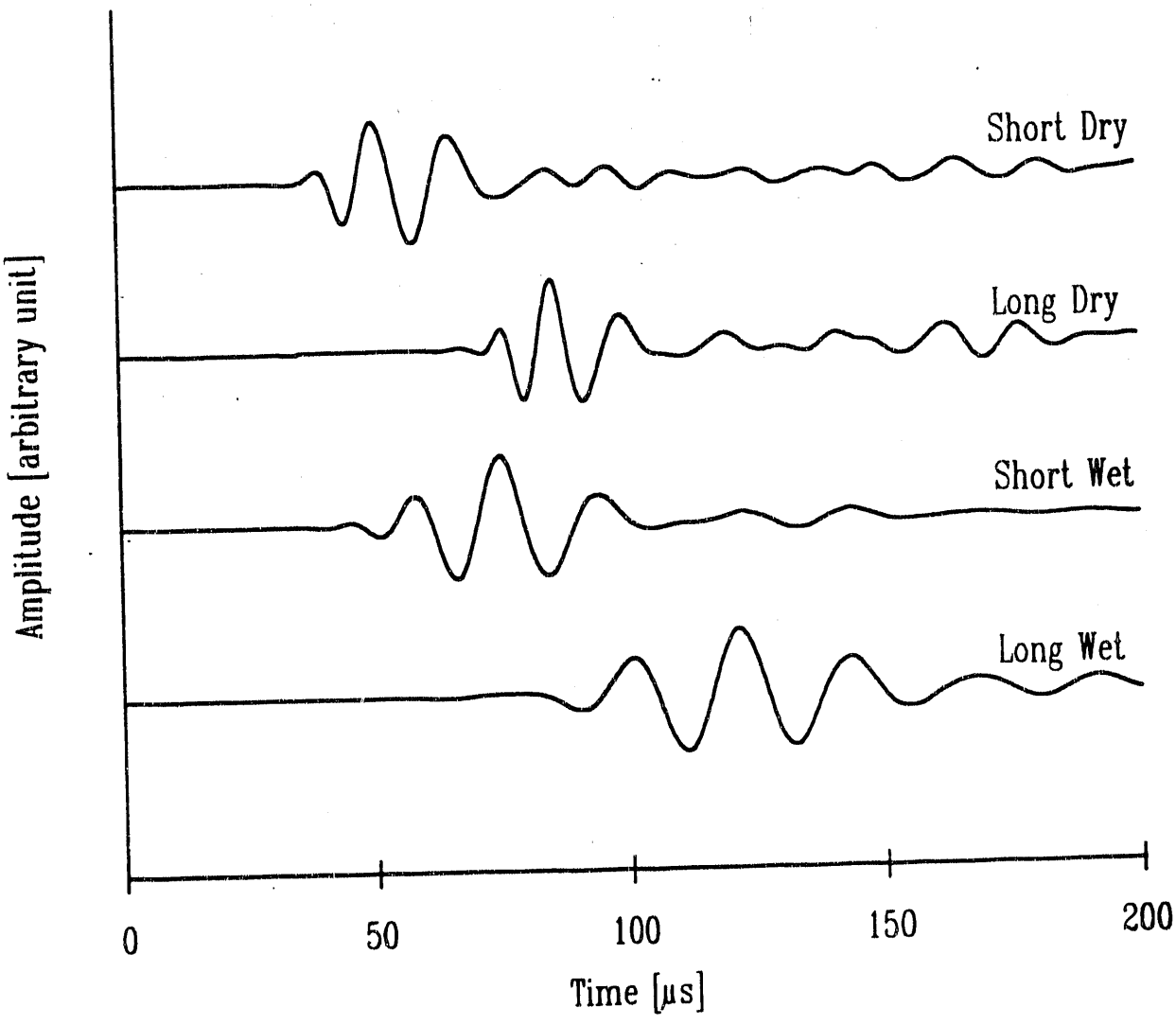

Figure 10 Surface wave signals on a Cavallo Buff Massillon Sandstone specimen in dry and wet conditions ("short" dimension: 1.9", "long" dimension: 3.8").

Table 3 Shear and surface wave velocities of different natural rocks.

Type	Origin	Velocity [m/s] shear dry	surface dry	surface wet
Berea Sandstone (100 mD)	Cleveland, Ohio	1530	1290	1290
Berea Sandstone (200 mD)	Cleveland, Ohio	1580	1410	1300
Berea Sandstone (300 mD)	Cleveland, Ohio	1450	1220	950
Berea Sandstone (450 mD)	Cleveland, Ohio	1470	1330	970
Massillon Sandstone (600 mD)	(LLNL)	1560	1460	1070
Cavallo Buff Massillon	Coshocton County, Ohio	1790	1490	1060
Sunset Blush Massillon	Coshocton County, Ohio	1620	1420	1010
Buff Limestone	Indiana	2510	2230	2210
Ledge Rock Sandstone	Tennessee	1960	1740	1740
McDermott Buff Sandstone	McDermott, Ohio	1300	1260	1030
Seneca Valley Sandstone	Brown County, Ohio	1510	1420	1250
Salt Creek Buff Limestone	Latham, Ohio	2810	2370	2130
McDermott Blue-Gray Sandstone	McDermott, Ohio	1570	1320	1060
Waverly Sandstone	Waverly, Ohio	1690	1670	1560
Berea Sandstone	Peninsula, Ohio	2360	2360	2000
Berea Sandstone	Warrensburg, Montana	1890	1800	1710

Figure 11 shows the Rayleigh velocity-to-shear velocity ratio for the first five samples of Table 3 (the permeabilities of these samples were measured at the Lawrence Livermore National Laboratory). There seems to be a weak trend of increasing ratio at higher permeabilities, which corresponds to an increasing Poisson's ratio. This would indicate weaker consolidation in the high-permeability samples, but the effect is not really significant since it is well below the experimental uncertainties indicated by the error bars. It should be mentioned that these error bars correspond to 7% combined uncertainty in the data, which, as for the ratio of the two velocities, might be a little too pessimistic. Some uncertainties present in the raw data (caused by inhomogeneity and anisotropy) cancel out in the comparison and the actual error might be well below 5%.

Figure 12 shows the ratio between the surface wave velocities in dry and wet samples as a function of permeability. The solid line is just an arbitrary fit to the experimental data to emphasize the trend of increasing ratio at higher permeabilities. The importance of these results lies in the relationship between fluid mobility and sound velocity. On the other hand, Figures 3 and 4 clearly demonstrated a similar effect between fluid mobility and surface wave attenuation, too. This aspect of the surface wave propagation along the free surface of a fluid-saturated rock needs to be further investigated. As an example Figure 13 shows the saturation induced attenuation increase in a Cavallo Buff Massillon Sandstone specimen. This is the difference between the attenuation spectra calculated from the time-domain signals shown in Figure 10 and it corresponds to added attenuation over a propagation length of 1.9". The induced attenuation is approximately one order of magnitude higher than in low-permeability rocks where the relative motion between the fluid and solid is negligible. It is also interesting to notice that the attenuation of this kind of surface wave seems to be proportional to the square of frequency while it is more like a linear relationship for the shear or ordinary Rayleigh waves.

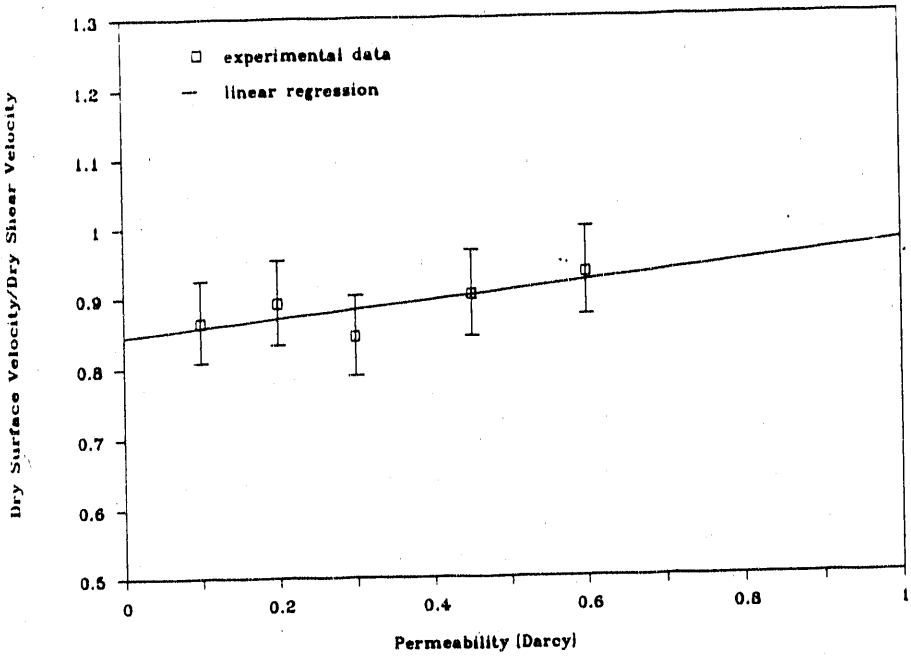

Figure 11 The ratio between the Rayleigh and shear velocities in dry rocks as a function of permeability.

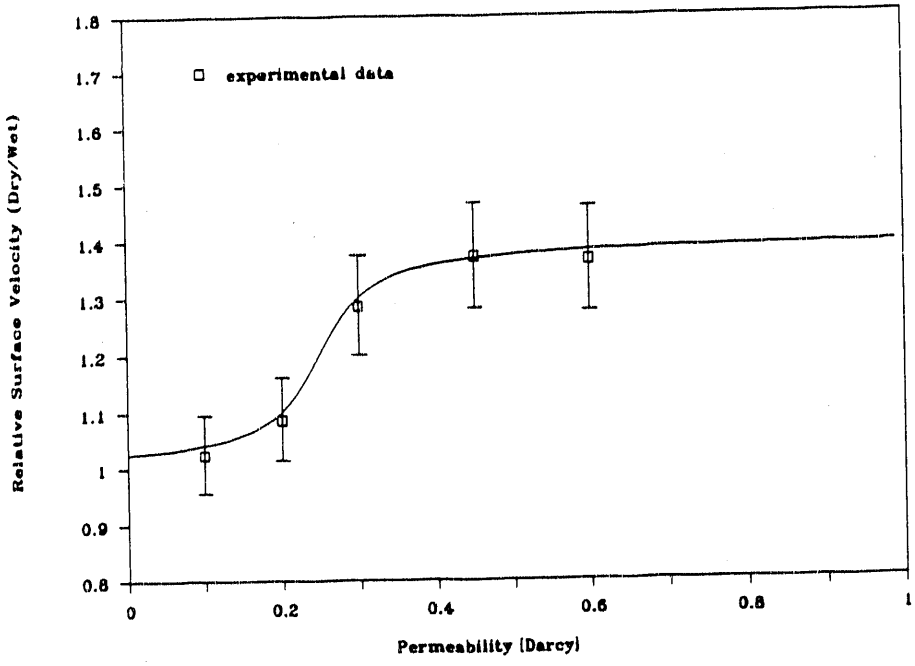

Figure 12 The ratio between the surface wave velocities in dry and wet samples as a function of permeability.

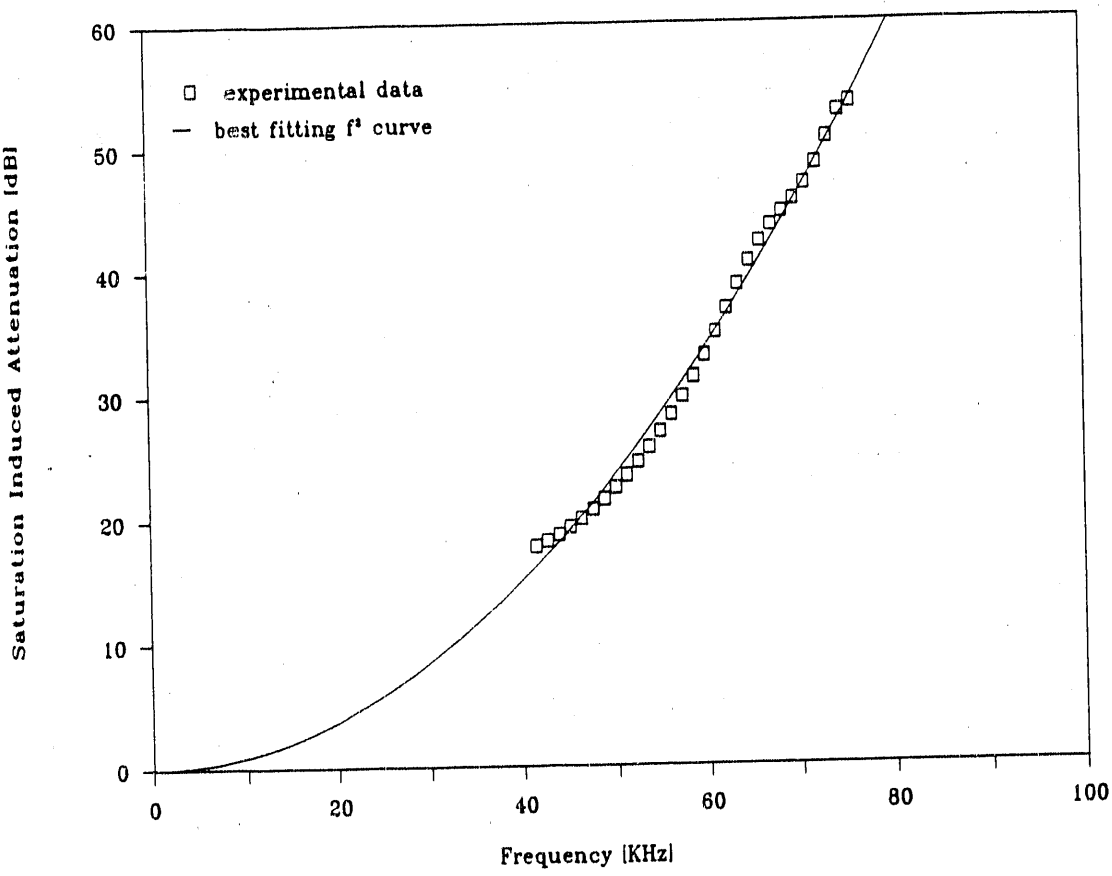

Figure 13 Saturation induced attenuation of the surface wave propagating along the free surface of a Cavallo Buff Massillon Sandstone specimen (propagation length: 1.9").

1.1.4 DISCUSSION AND CONCLUSIONS

Our research effort was based on the realization that, due to surface tension, practically closed-pore boundary conditions can prevail on the free surface of a water-saturated natural rock. We showed through the example of the true surface mode that approximately $T_s=10^7$ N/m^3 surface stiffness is sufficient to produce such conditions. This is significantly less than the $T_s=10^{11}$ N/m^3 value used by Feng and Johnson in their original calculations to model an ideally closed pore.[9] Our results are also in good agreement with the predictions of Wu at al.[17] They showed that the reflection coefficient from a water/water-saturated porous solid interface approaches its closed-pore asymptotic value above $T_s=10^7$ N/m^3, i.e., well before the four orders of magnitude higher value assumed by Feng and Johnson to make their numerical calculations more accurate.

Our calculations showed that capillary forces can easily produce closed-pore boundary conditions at the interface between a non-wetting fluid (air) and a porous solid saturated by a wetting fluid (water). The stiffness of the membrane extended over the surface pores depends on the surface tension of the wetting fluid and the pore size and shape. We derived a simple approximation relating the boundary stiffness to the formation permeability. We found that the boundary stiffness is around 10^{10} N/m^3 in most natural rocks, i.e., well above the threshold value required to achieve closed-pore boundary conditions. Under these conditions, the Rayleigh-type surface wave becomes strongly attenuated by energy leakage into the slow compressional wave and the velocity of the true surface mode drops below the slow wave velocity. Of course, the mobility of the water is badly limited by viscous drag between the fluid and the solid frame. This effect is particularly strong in natural rocks where the drag is greatly increased by inherent impurities such as submicron clay particles sticking to the pore walls and clogging the narrow throats of the pore channels. We modeled this effect in the usual

way by introducing a complex tortuosity which then describes both added inertia and viscous drag effects. We found that viscous loss increases both the velocity and the attenuation of the surface wave.

We used the direct excitation technique to measure surface wave velocity and attenuation on both wet and dry rocks. The Rayleigh velocity of dry rocks is approximately 10% lower than their shear velocity. The surface wave velocity of water-saturated rocks of low permeability (below 100-200 mD) is 5-10% lower than the Rayleigh velocity of the dry specimen. This drop in velocity is primarily due to the added inertia of the saturating fluid, which is also apparent in the similar decrease in the shear wave velocity. The surface wave velocity of water-saturated rocks of high permeability is much lower, approximately 60-70% of the Rayleigh velocity of the dry specimen. This strong correlation between the observed surface wave velocity change caused by water-saturation and the formation permeability can be used for ultrasonic assessment of the dynamic permeability. Further investigation is needed to establish a reliable theoretical model for the observed phenomenon and to develop inversion techniques for the quantitative evaluation of material properties from the velocity and attenuation of the surface wave propagating on the free surface of a fluid-saturated rock.

1.2 AIR-SATURATION TECHNIQUE

The most interesting feature of acoustic wave propagation in fluid-saturated porous media is the appearance of a second compressional wave, the so-called slow wave. The existence of a slow compressional wave in an isotropic and macroscopically homogeneous fluid-saturated porous medium was predicted by Biot in 1956.[18,19] The main characteristic of this mode is that its velocity is always lower than both compressional wave velocities in the fluid and solid frame. Below a critical frequency, which depends on the pore size in the frame and the kinematic viscosity of the fluid, the slow compressional wave is highly dispersive and strongly attenuated over a single wavelength. Above this critical frequency, it becomes a dispersion-free propagating wave with increasing but fairly low attenuation. The slow compressional wave represents a relative motion between the fluid and the solid frame. This motion is very sensitive to the kinematic viscosity of the fluid and the dynamic permeability of the porous formation. Naturally, low-viscosity liquids such as water are the fluids most often used in such experiments. In our current research effort, we have been studying the feasibility of using gaseous fluids such as air to saturate the porous specimens.

1.2.1 INTRODUCTION AND BACKGROUND

Since 1980, when Plona was able to observe slow wave propagation in artificial rocks made of sintered glass beads,[20] the question of why slow waves cannot be detected in real rocks has been one of the major issues in the acoustics of fluid-saturated materials. Recently, Klimenatos and McCann showed that this lack of perceivable slow wave propagation is probably due to inherent internal impurities, such as submicron clay particles, found in all types of natural rocks.[3] These clay particles,

deposited both within the pore throats and on the surfaces of the rock grains, greatly increase viscous drag between the fluid and solid frame, which results in excessive attenuation and usually complete disappearance of the slow wave. One way to reduce the excessive attenuation of slow waves in porous materials is to use special fluids of very low viscosity to saturate the specimen. For instance, superfluid ^{4}He below 1.1K has been shown to work very well in fused glass bead samples,[21] superleak materials consisting of compacted powders,[22-24] ands in sandstones,[25] but the technique is obviously very cumbersome.

The question of whether or not excessive attenuation in viscous fluid-saturated natural rocks renders the detection of slow waves impossible arises. Not necessarily! Even a very weak slow wave attenuated by as much as 50-60 dB could easily be detected but for the presence of much stronger background "noise" caused by the direct arrivals and scattered components of the fast compressional and/or shear waves. If we could generate a slow wave only and nothing else, it would be much easier to detect in spite of the substantial attenuation. Compared to the solid frame, liquids like water usually have a lower, but still comparable density ρ_f and bulk modulus B_f. Although their viscosity μ is also relatively high, which makes saturation of the porous sample somewhat troublesome, their kinematic viscosity $\eta=\mu/\rho_f$ is fairly low. On the other hand, gaseous fluids like air have very low density, bulk modulus, and viscosity as well, while their kinematic viscosity is usually rather high. Therefore, it is very simple to saturate a porous sample by air, but the slow wave is expected to be highly dispersive and strongly attenuated. In spite of these adverse effects, slow waves can be readily observed when an air-filled porous sample is insonified by airborne ultrasonic waves. Because of the tremendous acoustical mismatch between the incident compressional wave and the porous solid, all the energy is either reflected or transmitted via the slow wave without generating appreciable fast compressional or shear transmitted waves.

In order to demonstrate this crucial effect, Fig. 14 shows the slow, fast, and shear wave transmission coefficients through water and air-saturated glass bead specimens. The physical parameters of the glass bead specimen and details of the calculation are given in Ref. 17. In the case of water saturation, the slow compressional wave is usually 5-10 dB weaker than the fast compressional or shear modes and it is much more attenuated. Also, because of its slower velocity, it arrives later than the other modes and it is often overshadowed by multiple reflections and scattered components of these stronger signals. Maybe the only exception is when the shear velocity is sufficiently high so that we can work above the second critical angle where the slow compressional wave becomes the only propagating mode in the fluid-saturated sample. Unfortunately, this does not happen in most natural rocks where the shear velocity is rather low. On the other hand, in the case of air saturation, the slow compressional wave is at least 70 dB stronger than all other modes and, due to the very low sound velocity in air, the shear critical angle drops to below 15°, above which only the slow wave is transmitted through the sample. This means that a highly attenuated slow wave will be submerged in electrical noise rather than spurious signals so it can be easily recovered by simple time-averaging.

In spite of the excellent coupling between the incident compressional wave and the transmitted slow wave and the obvious advantage of saturating the specimen with low-viscosity air rather than high-viscosity water, slow wave propagation in air-filled porous samples has never been extensively studied in natural rocks. It should be mentioned that considerable work has been done on other air-filled porous materials at relatively low frequencies between 50 Hz and 4 kHz.[26-30] The apparent lack of interest is probably due to unusual technical difficulties associated with the generation and detection of airborne ultrasound and to the fact that slow waves are not expected to propagate in air-saturated porous samples as easily as in water-

a)

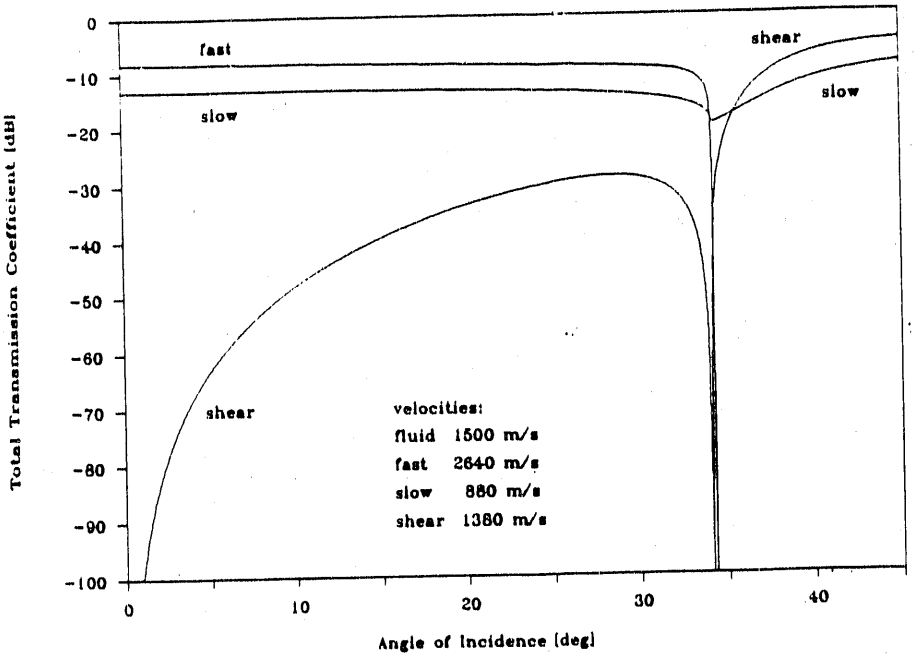

b)

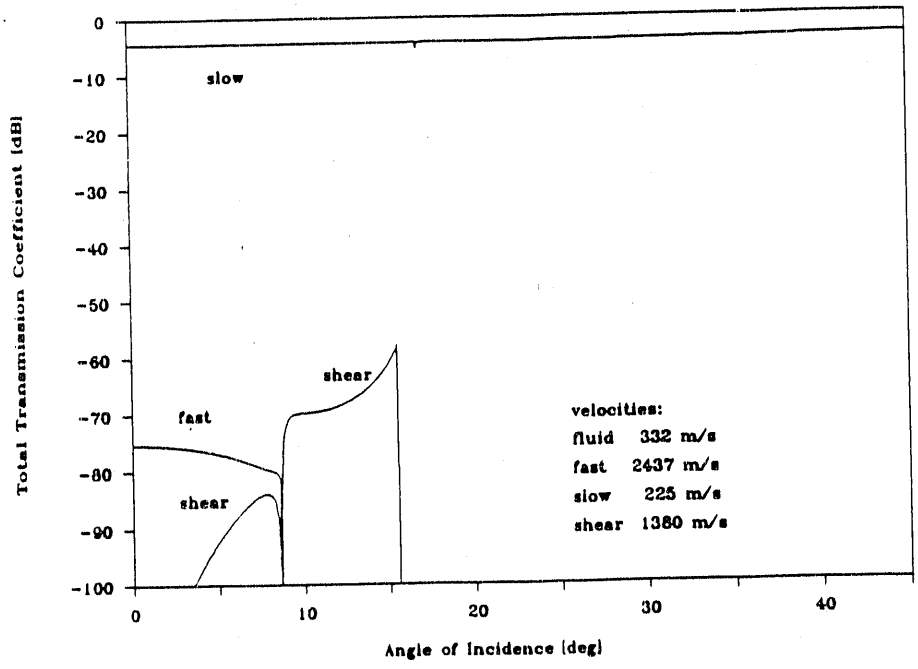

Figure 14 Slow, fast, and shear transmission coefficients through (a) water- and (b) air-saturated porous glass bead plates.

saturated ones[1]. Since the kinematic viscosity of air is so large and the velocity of sound in air is so small, there is but a very narrow frequency window where the attenuation coefficient is sufficiently low to observe a dispersion-free, scattering-free slow wave. This "window" is set by the conditions that the viscous skin depth $\delta=(2\eta/\omega)^{1/2}$ be less than the pore size a_p and, simultaneously, the wavelength λ be larger than the grain size a_g. Table 4 summarizes the relevant physical parameters of water and air as well as f_{min} and f_{max}, i.e., the limits of the frequency window where slow wave propagation is expected. a_g=200μm grain diameter and ϕ=30% porosity were assumed in the calculations. The slow wave velocity at high frequencies can be easily calculated by assuming a perfectly stiff frame as $v=v_f/\tau^{1/2}$, while the tortuosity τ can be estimated from the porosity ϕ as $\tau=1/2\ (\phi^{-1}+1)$.[31] To determine f_{min} and f_{max}, we assumed that the pore size is approximately 15% of the grain size and at least four times larger than the viscous skin depth to account for the smaller cross sections at the crucial pore throats:

$$f_{min} = \eta/\pi(0.04a_g)^2 \qquad (17.a)$$

and

$$f_{max} = v/2\pi a_g. \qquad (17.b)$$

Table 4 clearly demonstrates the greatly reduced frequency window where dispersion-free and (more or less) attenuation-free slow wave propagation can be expected in air-filled samples of approximately 200μm grain size. On the other hand, these results do not exclude slow wave propagation over a much larger frequency range. They simply mean that the slow wave becomes increasingly dispersive below 100 kHz and very strong attenuation can be expected above 200 kHz.

Table 4 Physical parameters of water and air at 20°C.

	ρ_f (kg/m^3)	v_f (m/s)	η (mm^2/s)	f_{min} (kHz)	f_{max} (kHz)
Water	1000	1480	1	5	810
Air	1.3	332	15	75	180

1.2.2 ANALYTICAL RESULTS

For the special case of air-saturated permeable solids of random formation, Attenborough's theoretical model[29] can be used to determine both the complex wave number k and the complex acoustic impedance Z:

$$k(\omega) = \omega[\rho(\omega)/K(\omega)]^{1/2}, \qquad (18.a)$$

and

$$Z(\omega) = [\rho(\omega)K(\omega)]^{1/2}, \qquad (18.b)$$

where ρ and K denote the complex density and the complex modulus, respectively, of the air-saturated material. The complex density includes the effect of viscosity

$$\rho(\omega) = \rho_f \tau_\infty/\phi[1-T(\xi)], \qquad (19.a)$$

while the complex modulus includes the somewhat weaker effect of heat conduction in air

$$K(\omega) = K_f/\phi[1+(\gamma-1)T(Pr^{1/2}\xi)]. \qquad (19.b)$$

γ denotes the specific heat ratio ($\approx$1.4 for air) and Pr is the Prandtl number ($\approx$0.74 for air). T is a simple function of the normalized pore radius ξ:

$$T(\xi) = 2J_1([-i]^{1/2}\xi)/([-i]^{1/2}\xi)J_0([-i]^{1/2}\xi), \qquad (20.a)$$

where J_o and J_1 are the zero- and first-order Bessel functions and i is the imaginary unit. For cylindrical tubes, the normalized pore radius is exactly known:

$$\xi = a\ (\omega/\eta)^{1/2}, \qquad (20.b)$$

where a denotes the actual pore radius. For real porous materials of random pore geometry, there is no corresponding exact solution. Attenborough[29] suggested that the normalized pore radius should be calculated as

$$\xi = (2\tau_\infty \kappa_o \omega/\phi\eta s_p^2)^{1/2}, \qquad (20.c)$$

where κ_o is the static permeability, τ_∞ is the high-frequency tortuosity, and s_p is the so-called pore shape factor ratio which is usually between 0.1 and 0.5.

This analytical technique provides a unified model for both low-frequency (diffuse) and high-frequency (propagating) regimes of the slow compressional wave in air-saturated porous solids. It uses four basic parameters, namely porosity (ϕ), high-frequency tortuosity (τ_∞), static permeability (κ_o), and pore shape factor ratio (s_p), to describe the porous formation. We chose it instead of the previously mentioned dynamic permeability model of Johnson et al.[14] because the later one is limited to fluids of negligible thermal expansion coefficient. Comparison of the two models reveals that the actual difference between them is rather small. The best agreement can be achieved by asymptotic matching of Equations 15, 16 and 19-21. From the low- and high-frequency asymptotes, we get identical results if $s_p = \gamma^{1/2} \approx 0.423$ and $\Lambda \approx (5.6\ \tau_\infty \kappa_o/\phi)^{1/2}$. As an example, Figure 15 shows the calculated attenuation coefficient of the slow compressional wave in a porous solid of $\phi = 0.3$, $\tau_\infty = 1.79$, $\kappa_o = 2.2\ 10^{-12} m^{-2}$, and $s_p = 0.423$. The largest discrepancy between the two models occurs at the transition between the diffuse and propagating regimes, but it never exceeds 12%.

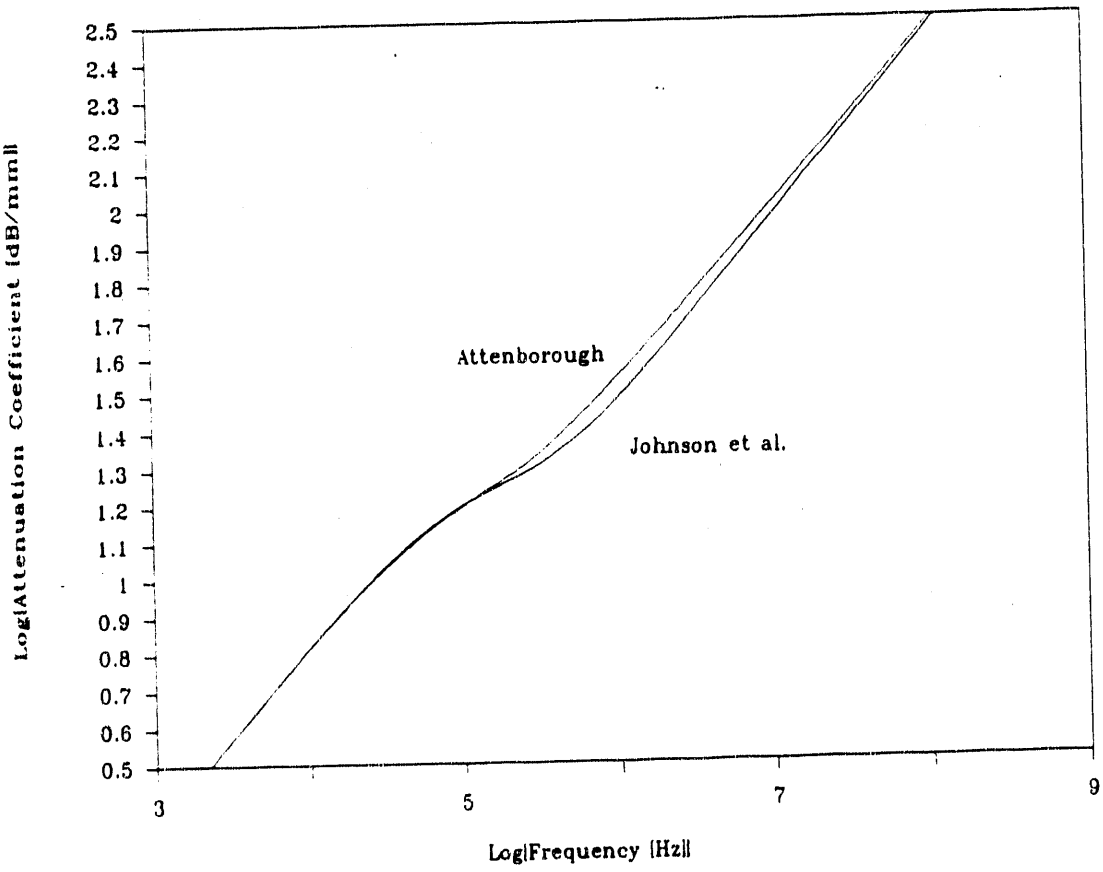

Figure 15 Comparison between the two different slow wave propagation models of Attenborough[29] and Johnson et al.[14]

Since the static permeability κ_o and the pore shape factor ratio s_p always occur in the same combination through the normalized pore radius ξ, they cannot be separated by acoustical measurements. According to the dynamic permeability theory of Johnson et al.,[14] at low frequencies, the complex wave number of the slow compressional wave can be approximated as

$$k^{(low)} = k_f(i\phi\eta/\kappa_o\omega)^{1/2}. \tag{21a}$$

Attenborough's model yields a similar form of

$$k^{(low)} = k_f(i\phi\eta/\kappa_a\omega)^{1/2}, \tag{21b}$$

where κ_a denotes the acoustic permeability:

$$\kappa_a = \kappa_o/4\gamma s_p^2. \tag{21c}$$

Only three independent parameters can be determined from acoustic measurements on air-filled porous solids: porosity ϕ, high-frequency tortuosity r_∞, and the low-frequency acoustic permeability κ_a, which is a combination of the static permeability κ_o and the pore shape factor ratio s_p. s_p is always less than 0.5 while γ is higher than one for gases. As we mentioned above, the acoustic permeability equals the static one for s_p=0.423. For cylindrical pores, the pore shape factor ratio reaches its maximum of s_p=0.5 and the acoustic permeability is slightly lower than the static permeability. This is because the specific heat ratio is higher than one in air and the slow wave velocity depends on the isothermal sound velocity $v_T=v_f/\gamma^{1/2}$ rather than on the adiabatic velocity which is measured in an infinite medium. For pores with non-circular cross-sections, the pore shape factor ratio s_p can be much lower than 0.5. For example, in the case of equilateral triangle cross-section, s_p is as low as 0.158.[29] We shall show that, in the case of natural rocks, the pore shape factor ratio is usually between 0.2 and 0.4, therefore the acoustic permeability is somewhat higher than

the static one.

In order to demonstrate the main features of slow wave propagation in air-filled porous solids, we used Attenborough's technique to calculate the sound velocity and attenuation as well as the complex acoustic impedance in sintered glass bead specimens of different grades. Table 5 lists the material parameters used in these calculations. The porosity and static permeability were obtained from the manufacturer's (Eaton Products International, Inc.) specifications. The high-frequency tortuosity was taken from Ref.1 as the parameter giving the best agreement between experimental measurements and theoretical predictions for the slow wave velocity in water-saturated sintered glass bead samples. This value is very close to other published data on similar materials.[21,32,33] Finally, the pore shape factor ratios were chosen by matching the analytical results to our experimental data to be presented in the next chapter.

Table 5 Material parameters of sintered glass bead specimens.

Grade	ϕ	$\kappa_o[10^{-12}m^{-2}]$	τ_∞	s_p
15	0.3	2.2	1.79	0.460
40	0.3	6.5	1.79	0.460
55	0.3	11.0	1.79	0.475
90	0.3	27.0	1.79	0.475
175	0.3	67.0	1.79	0.475

Figure 16 shows the normalized velocity v/v_f and the attenuation coefficient of the slow compressional wave in the air-filled porous samples listed in Table 5 as functions of frequency. In the diffuse regime, i.e., at low frequencies, both the velocity and the attenuation coefficient are proportional to the square-root of frequency:

a)

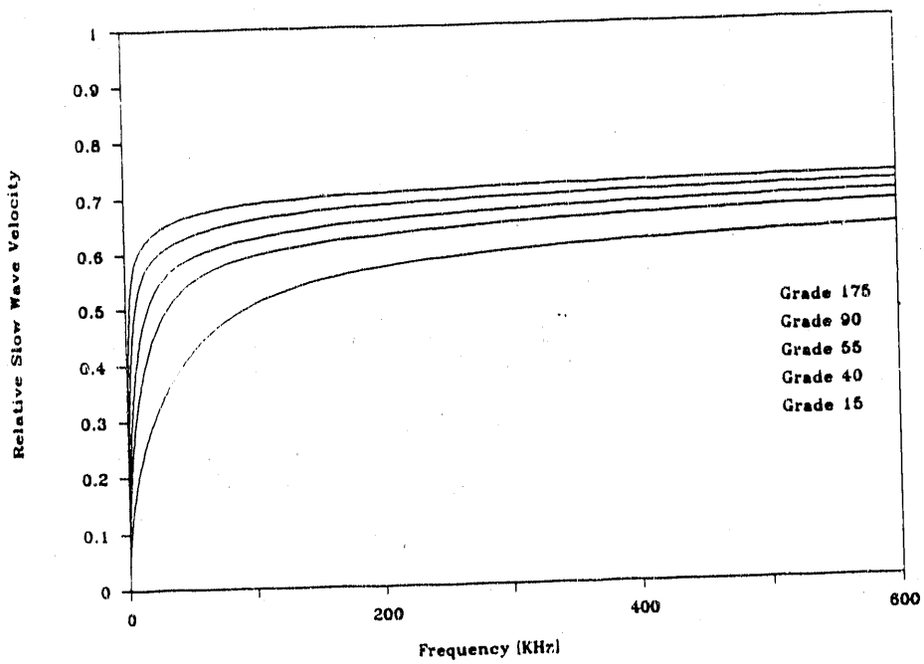

b)

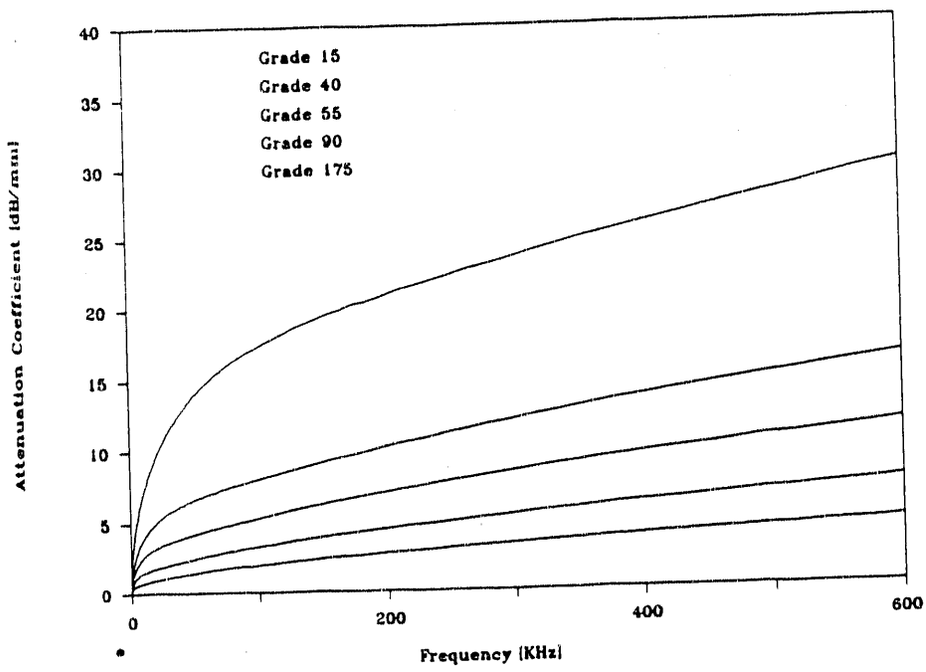

Figure 16 Normalized velocity (a) and attenuation coefficient (b) of the slow compressional wave in air-filled sintered glass bead specimens as a function of frequency for different grades.

$$v^{(low)}/v_f = (\omega\kappa_o/2\eta\phi\gamma s_p^2)^{1/2} \qquad (22.a)$$

and

$$\alpha^{(low)} = (2\omega\eta\phi\gamma s_p^2/\kappa_o v_f^2)^{1/2}, \qquad (22.b)$$

therefore the normalized attenuation coefficient α_n, i.e., the total attenuation over one wavelength, is constant

$$\alpha_n^{(low)} = \alpha\ v/f = 2\pi\ [\text{Neper}] \approx 55\ \text{dB}. \qquad (22.c)$$

In the propagating regime, i.e., at high frequencies, the velocity approaches a constant value while the attenuation coefficient remains proportional to the square-root of frequency, although the proportionality coefficient is slightly different from the low-frequency value (see Figure 15).

$$v^{(high)}/v_f = \tau_\infty^{-1/2} \qquad (22.d)$$

and

$$\alpha^{(high)} = (\omega\eta\phi\tau_\infty s_p^2/4v_f^2\kappa_o)^{1/2}[1+(\gamma-1)/Pr^{1/2})], \qquad (22.e)$$

where the second term of Equation 22.e is approximately 1.46 for air. It is interesting to note that the ratio between the high- and low-frequency asymptotic values of the attenuation coefficients is

$$\alpha^{(high)}/\alpha^{(low)} \approx 0.43\ \tau_\infty^{1/2}, \qquad (22.f)$$

i.e., fairly close to one for most porous solids of interest to us. Of course, in the propagating regime, the normalized attenuation coefficient decreases with frequency, at least to a point where other attenuation mechanisms such as scattering are still negligible.

Figure 17 shows the real and imaginary components of the

acoustic impedance in air-filled sintered glass bead specimens as functions of frequency for five different grades. Both components were normalized to the acoustic impedance of the saturating air, $Z_f = v_f \rho_f$. At low frequencies, the moduli of both components are very large and decreasing with frequency. At high frequencies, the real part approaches a finite asymptotic value

$$Z^{(high)}/Z_f = \tau_\infty^{1/2}/\phi, \qquad (23)$$

while the imaginary part diminishes.

In the diffuse regime, where transmission-type measurements are not feasible because of the very high normalized attenuation coefficient, we have to rely on determining the complex acoustic impedance from reflection-type measurements. In the propagating regime we can use transmission measurements to determine the velocity and attenuation coefficient of the slow compressional wave. Even then, but especially in the transition region between the diffuse and propagating regimes, we have to take into account the total transmission loss T_o caused by the significant acoustical impedance mismatch between the air and the air-filled specimen:

$$T_o = 4/(2+Z/Z_f+Z_f/Z). \qquad (24)$$

The easiest thing to do is to approximate the actual acoustic impedance by its real-valued high-frequency asymptote. For example, $T_o^{(high)} \approx -4.5$ dB for $\phi = 0.3$ and $\tau_\infty = 1.79$. In this way, we inevitably underestimate the total transmission loss and, consequently, overestimate the attenuation coefficient. Also, because of the phase-shift caused by the complex nature of T_o, we slightly underestimate the slow wave velocity in samples of small thickness. In order to get better agreement between experimental measurements and theoretical calculations, we can easily correct our analytical results for the difference between the actual transmission loss T_o and its real valued asymptote $T_o^{(high)}$.

a)

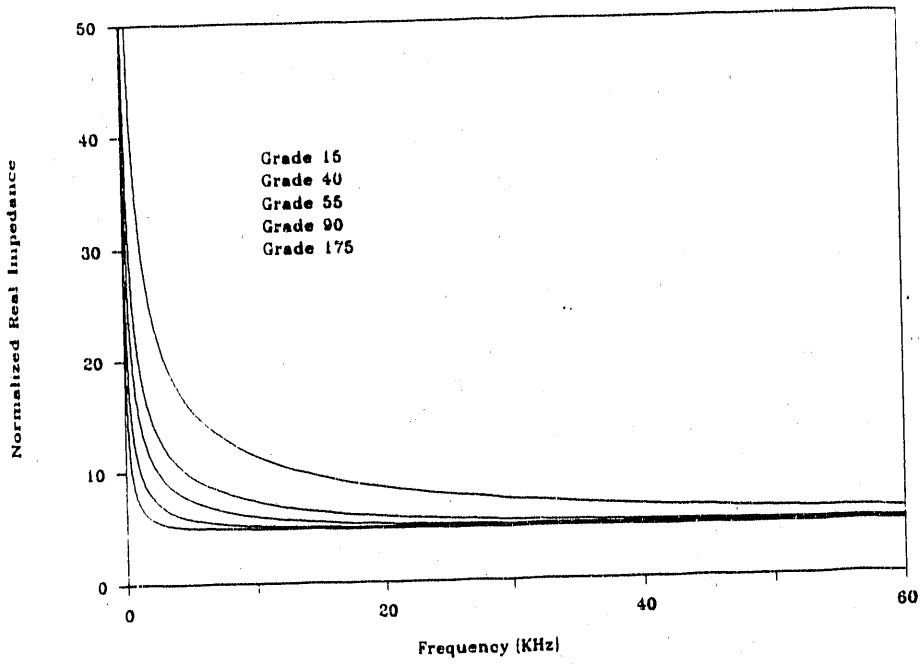

b)

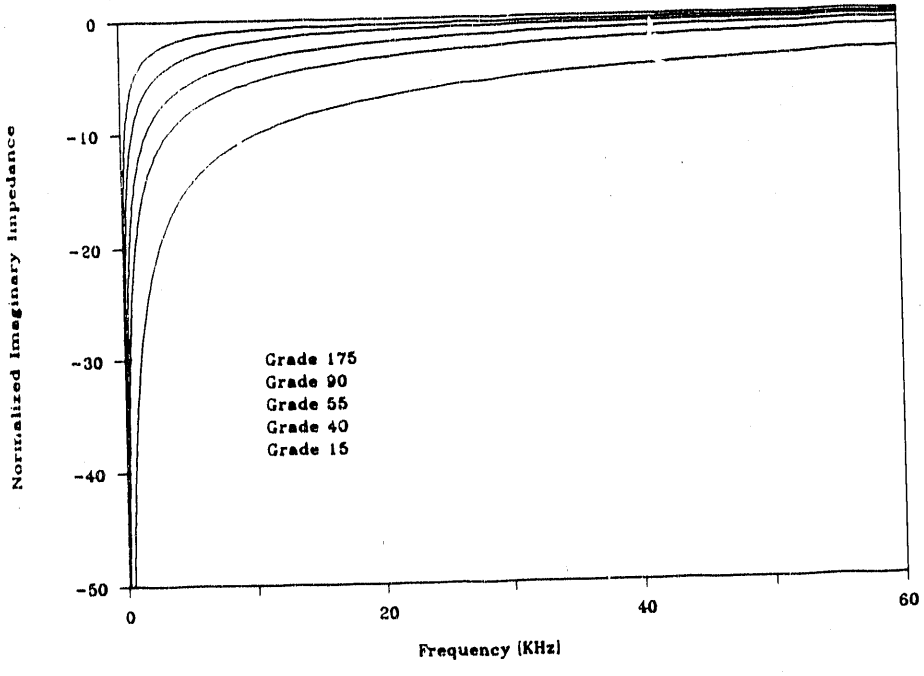

Figure 17 Normalized real (a) and imaginary (b) components of the acoustic impedance in air-filled sintered glass bead specimens as functions of for different grades.

The measured transmission coefficient frequency

$$T_m(\omega) = T_o(\omega)\ \exp(i\omega d/v)\ \exp(-\alpha d) \qquad (25.a)$$

can be expressed as

$$T_m(\omega) = T_o^{(high)}(\omega)\ \exp(i\omega d/v_a)\ \exp(-\alpha_a d), \qquad (25.b)$$

where d is the thickness of the specimen and v_a and α_a are the apparent velocity and attenuation coefficient, which are corrected according to d. Figure 18 shows the apparent velocity and attenuation coefficient of the slow compressional wave in air-filled sintered glass bead specimen Grade 55 as functions of frequency for different sample thicknesses. Because of the larger impedance mismatch and the additional phase-shift at lower frequencies, the apparent velocity drops while the apparent attenuation increases in thin samples. In the propagating regime (above $\approx$ 60 kHz), the corrections are negligible. In the next chapter, we are going to compare our experimental data to such corrected analytical results.

a)

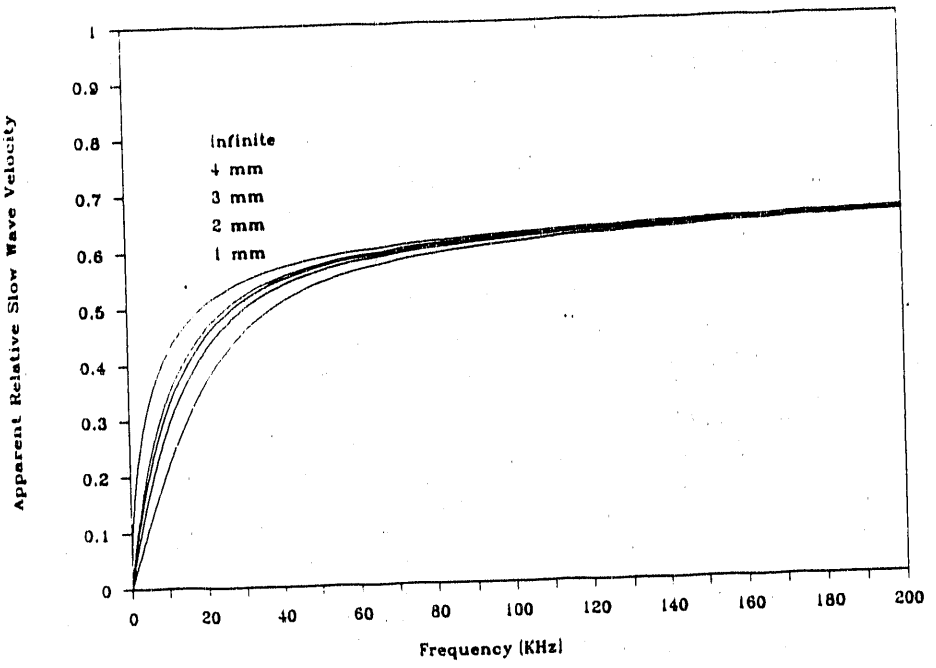

b)

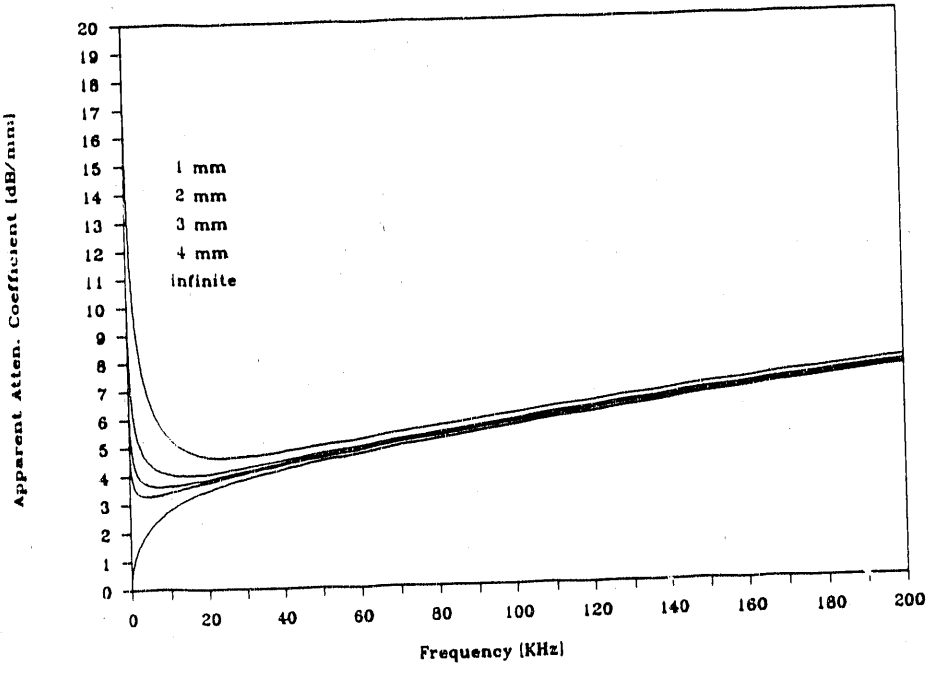

Figure 18 Apparent velocity (a) and attenuation coefficient (b) of the slow compressional wave in air-filled sintered glass bead specimen Grade 55 as a function of frequency for different sample thicknesses.

1.2.3 EXPERIMENTAL TECHNIQUE AND RESULTS

Figure 19 shows the block diagram of the experimental system used in this study. It is based on our recently developed method using the transmission of airborne ultrasonic waves through thin plates of air-filled porous specimens to investigate the propagation parameters of the slow compressional wave.[34] Standard ultrasonic NDE equipment was used without any particular effort to obtain high generation or detection sensitivity. The rather poor coupling between the applied contact transducers and air resulted in a rather low, but fairly constant, sensitivity over a wide frequency range of 50-500 kHz. In the case of necessity, we replaced the ultrasonic transmitter and receiver by a commercial tweeter and electret microphone so that measurements could be done between 10 kHz and 50 kHz, too. In order to assure an acceptable signal-to-noise ratio, extensive signal averaging was used, up to 10^5 samples. The transmitter was driven by a tone-burst of five cycles. The received signals with and without the specimen placed between the transducers were digitally stored. Then the computer selected the first five cycles of the signal, from which the computer determined the insertion loss L_i and insertion delay T_i. The insertion loss was calculated by Fourier transforming the gated signals and calculating the ratio between the maximum amplitudes in the two spectra. The insertion delay was determined by finding the maximum of the cross-correlation function of the two signals. Finally, the apparent attenuation coefficient and normalized velocity were calculated as

$$\alpha_a = (L_i - T_o)/d \qquad (26.a)$$

and

$$v_a/v_f = 1/(1+T_i v_f/d), \qquad (26.b)$$

respectively. The thicknesses of the specimens were varied between 1 and 5 mm to accommodate different permeabilities over the widest possible frequency range.

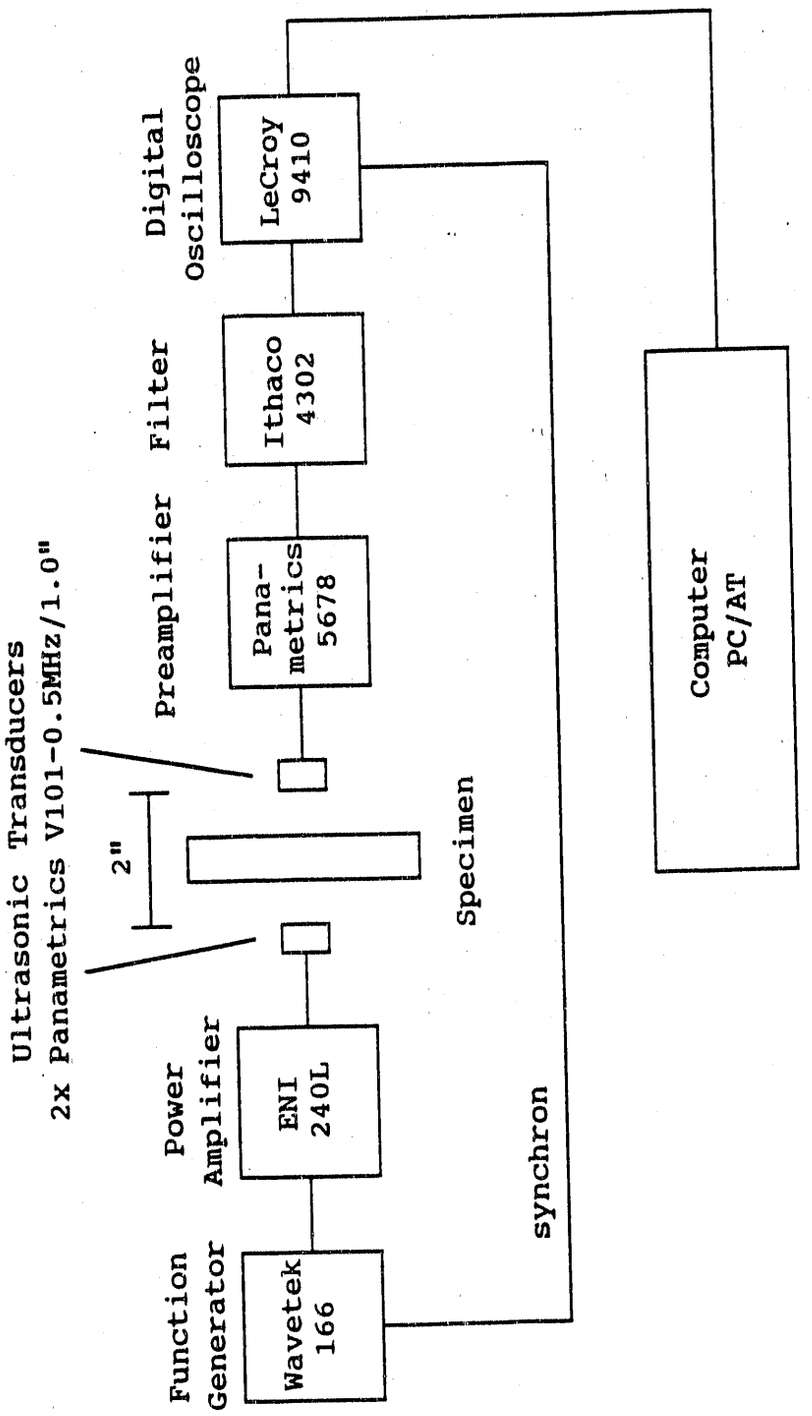

Figure 19 Block diagram of the experimental system.

Measurements were made on different ceramic, metallic, and polymer filter materials as well as natural rocks. First, let us show some typical results on synthetic materials of well-defined porous structure to demonstrate the accuracy of the measurement. Second, we shall present similar results on different natural rocks of much more complicated pore structure to demonstrate the feasibility of the developed technique for ultrasonic evaluation of such less-permeable formations.

The first series of experiments were conducted on sintered glass bead specimens listed above in Table 5. Generally, we found very good agreement between the theoretically predicted and experimentally measured slow wave velocities. As an example, Figure 20 shows the comparison between the theoretical and experimental results for Grades 55 and 90. For the attenuation coefficient, the agreement is less perfect. Figure 21 shows the comparison between the theoretical and experimental results for Grades 15 through 175. For the smallest pore size (Grade 15) the agreement is still acceptable indicating that the total attenuation is dominated by viscous losses throughout the whole frequency range. As the pore size is gradually increased, at first only at higher frequencies (Grades 40 and 55) then throughout the whole frequency range (Grades 90 and 175), viscous losses drop below scattering losses and the attenuation coefficient approaches a linear asymptote (dashed-lines in Figure 20.b-e). The same behavior was also observed in other synthetic materials such as sintered steel and bronze specimens.

a) Grade 55

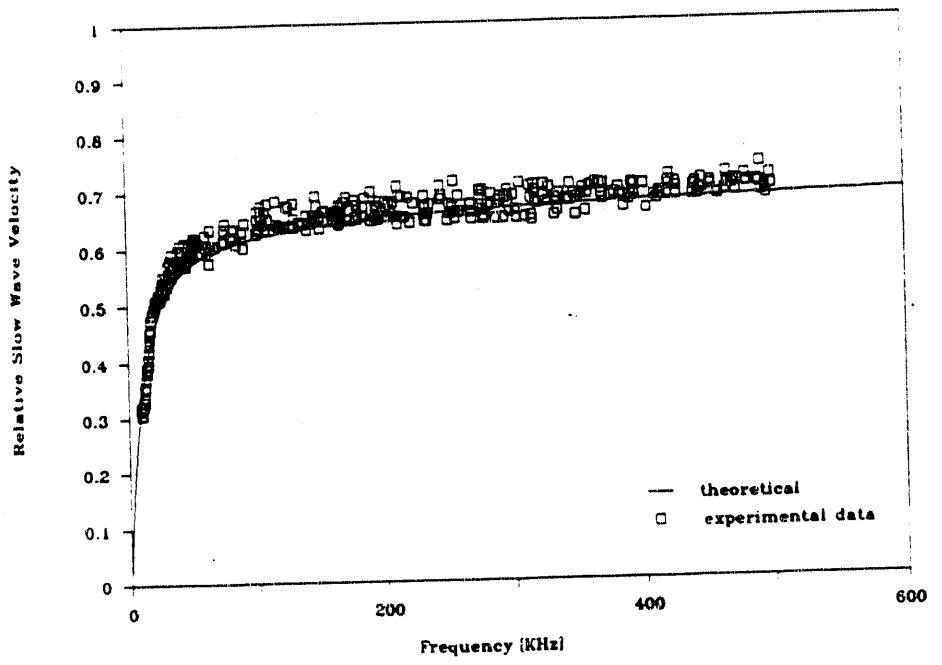

b) Grade 90

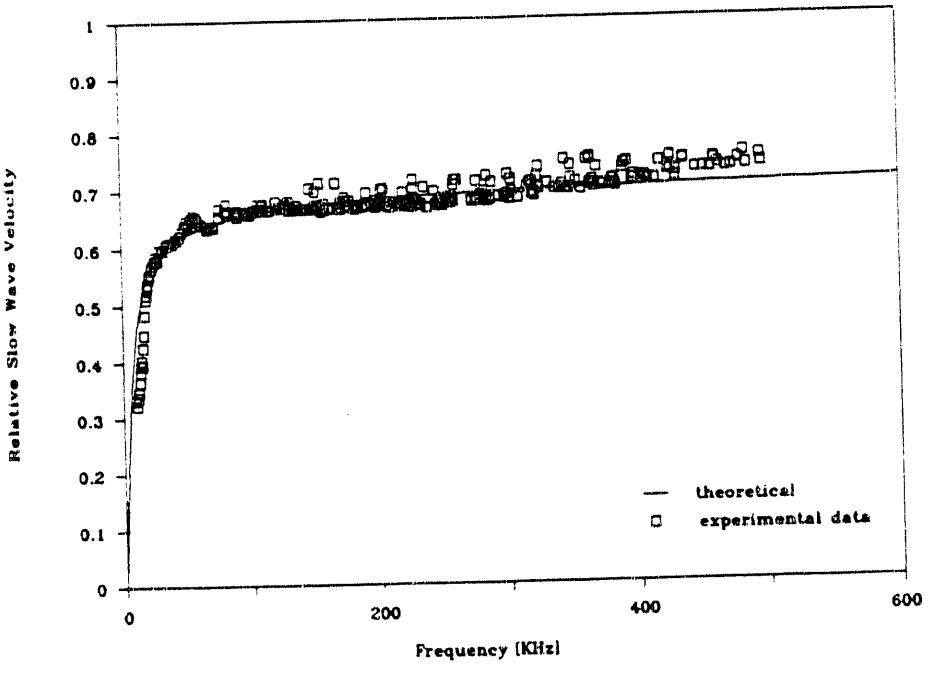

Figure 20 Comparison between the theoretically predicted and experimentally measured slow wave velocities in sintered glass bead specimens for Grades 55 (a) and 90 (b).

a) Grade 15

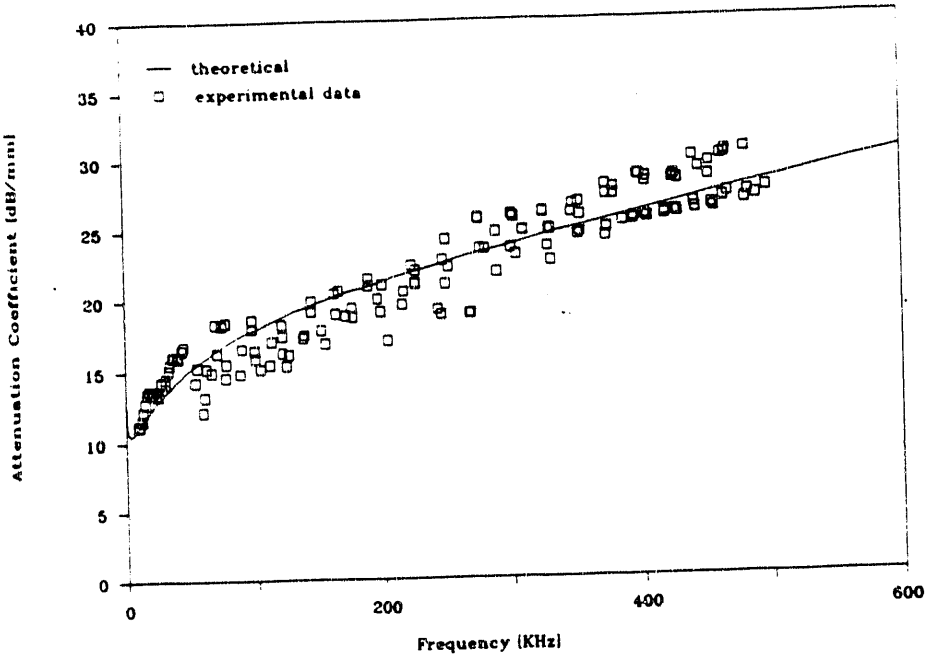

b) Grade 40

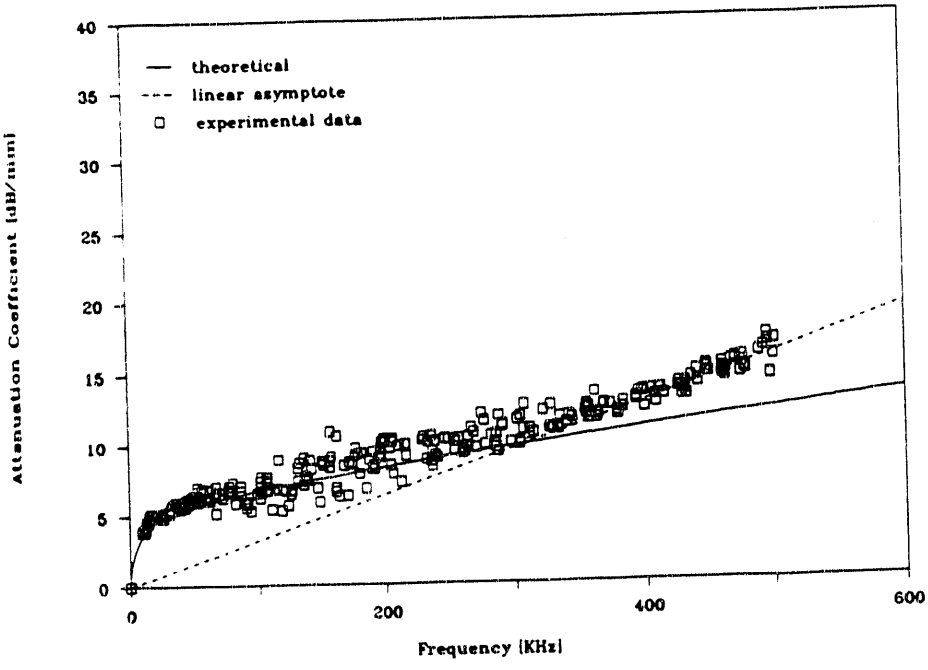

Figure 21a,b Comparison between the theoretically predicted and experimentally measured slow wave attenuations in sintered glass bead specimens for Grades 15 (a) and 40 (b).

c) Grade 55

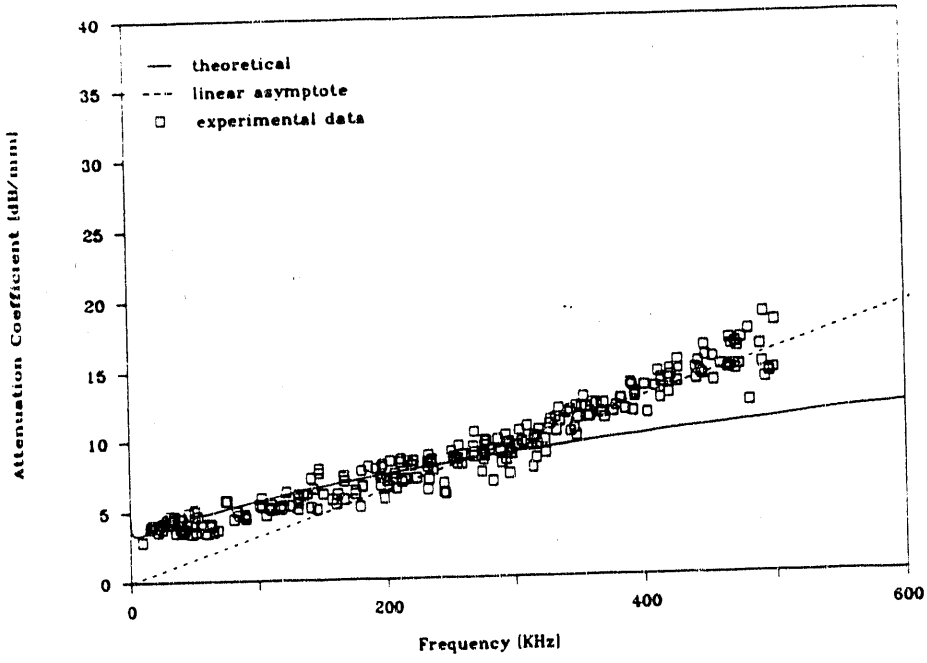

d) Grade 90

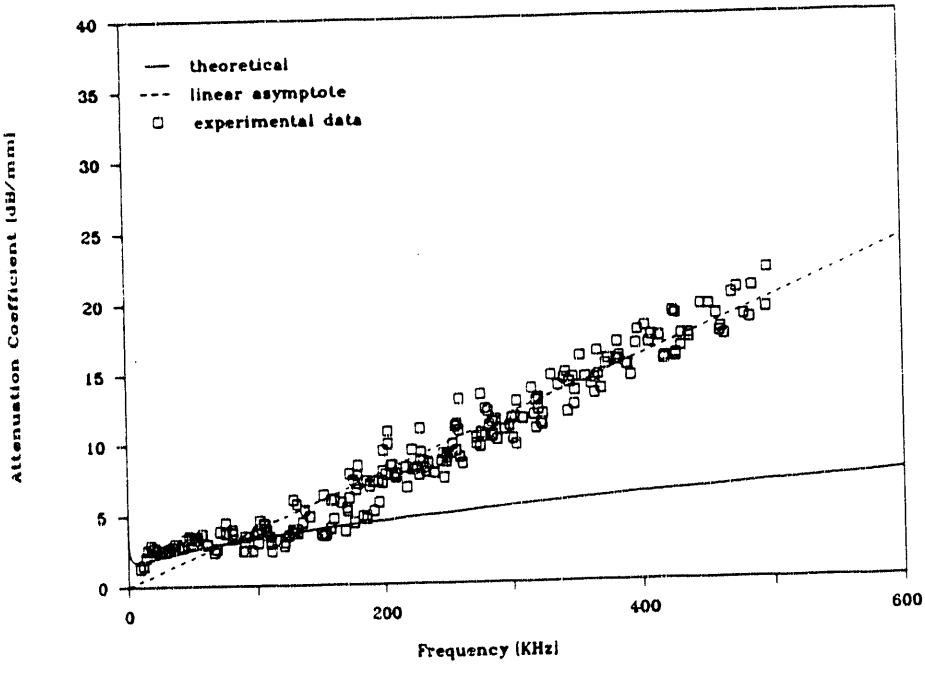

Figure 21c,d Comparison between the theoretically predicted and experimentally measured slow wave attenuations in sintered glass bead specimens for Grades 55 (c) and 90 (d).

e) Grade 175

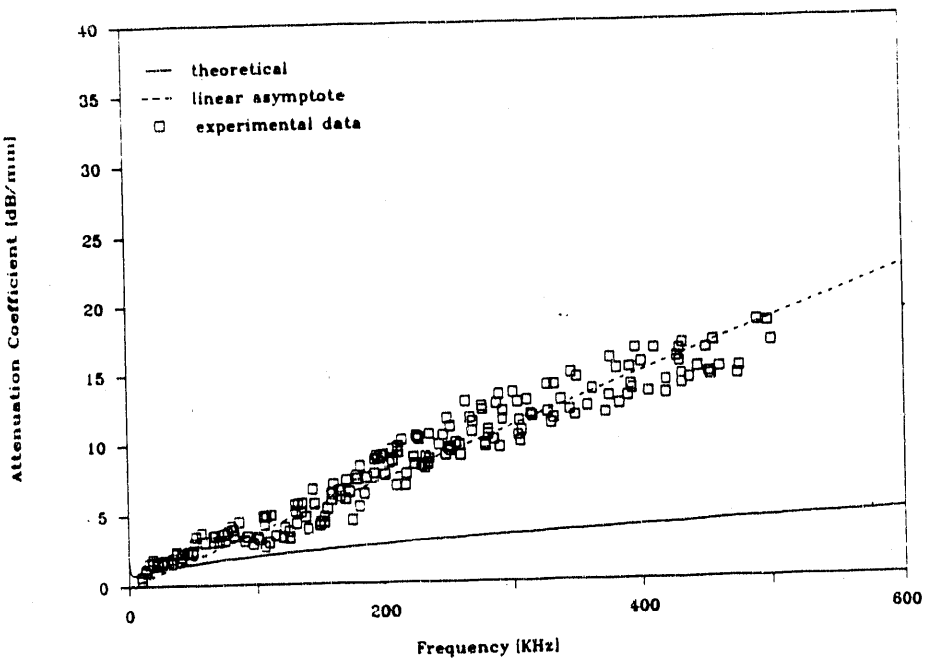

Figure 21e Comparison between the theoretically predicted and experimentally measured slow wave attenuations in sintered glass bead specimens for Grade 175.

The primary purpose of our experiments on synthetic porous materials was to improve the accuracy of the measuring system and to verify the feasibility of Attenborough's simple model for random but statistically relatively well-defined permeable formations. Naturally, our next step was the adaptation of this technique to natural rocks of relatively high permeability between 100 and 1000 mD. Basically, the results were fairly similar to those obtained for synthetic materials, although the scatter of the data became somewhat larger due to inherent macroscopic inhomogeneities found in most natural porous materials. Table 6 lists the materials used in this part of the study as well as their relevant properties. With the exception of the permeability of the Berea Sandstone specimen, which was measured at the Lawrence Livermore National Laboratory, all parameters were adjusted to obtain the best agreement between the analytical results and the experimental data. Later we plan to determine the three basic material parameters, namely the porosity, the permeability, and the tortuosity, by separate measurements and adjust only the pore shape factor ratio, which is the only truly independent acoustic parameter.

Table 6 Material parameters of natural rocks.

Type	ϕ	κ_o $[10^{-12}m^{-2}]$	τ_∞	s_p	d [mm]
Cavallo Buff Massillon	0.15	0.7	2.6	0.3	2.4
Sunset Blush Massillon	0.15	0.6	2.8	0.3	2.1
Cu Variegated Sandstone	0.13	0.6	2.3	0.3	1.7
Berea Sandstone	0.12	0.2	3.2	0.2	1.5

Figures 22-25 show the normalized slow wave velocity and total insertion loss in different natural rock specimens. Again, the experimentally measured velocity agrees very well with the analytical results while the attenuation exhibits higher-than-predicted attenuation and more or less linear frequency dependence. The samples were approximately 4" in diameter and showed significant inhomogeneity of the attenuation distribution within this area. Because of the very high attenuation in these samples, resonance peaks in the transmission are generally very weak but sometimes, especially at lower frequencies, faintly visible.

a)

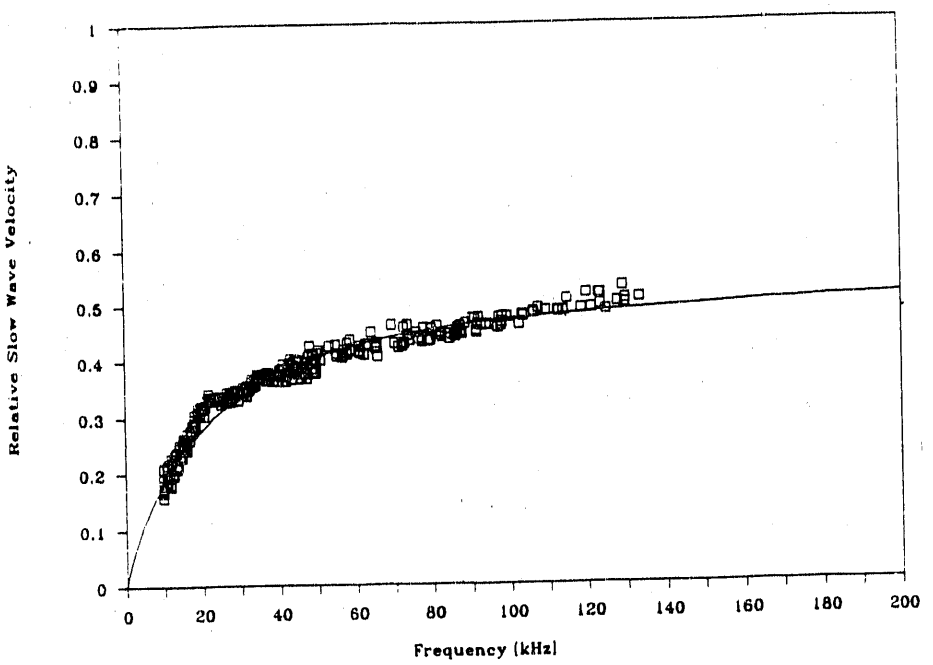

b)

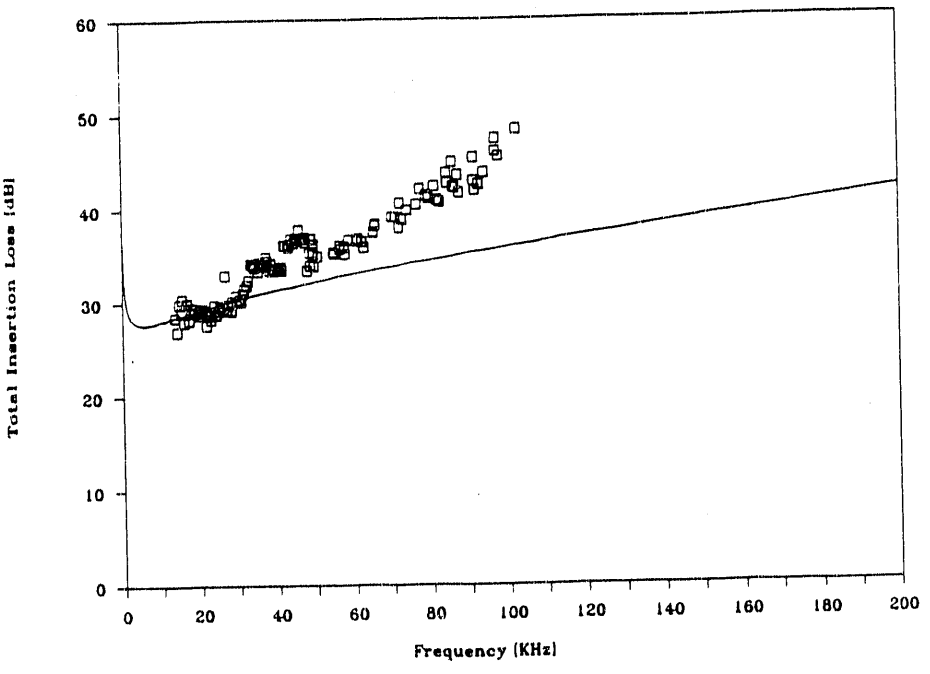

Figure 22 Normalized slow wave velocity and total insertion loss in a 2.4-mm-thick Cavallo Buff Massillon Sandstone specimen.

a)

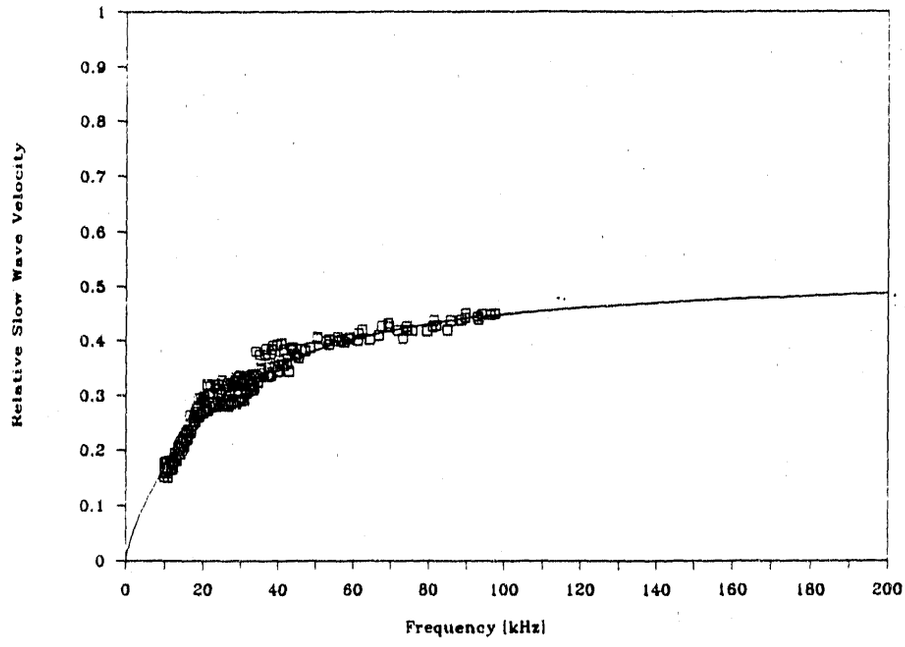

b)

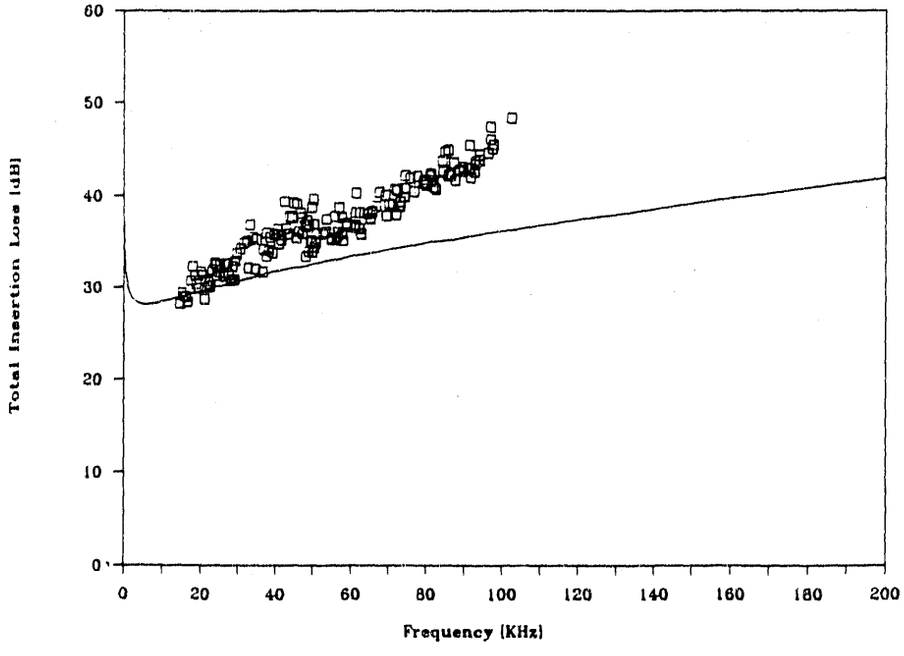

Figure 23 Normalized slow wave velocity and total insertion loss in a 2.1-mm-thick Sunset Blush Massillon Sandstone specimen.

a)

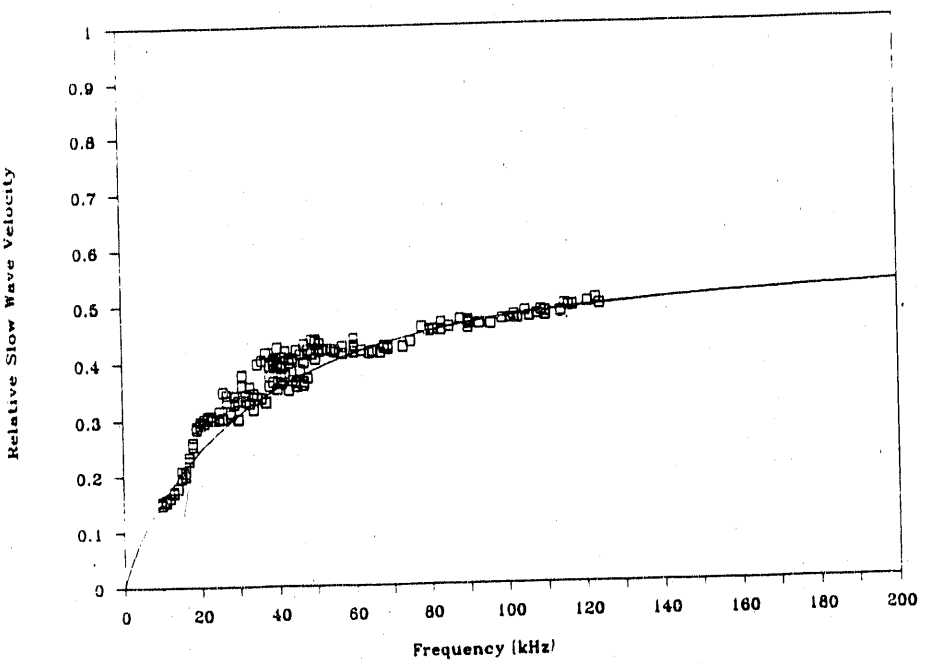

b)

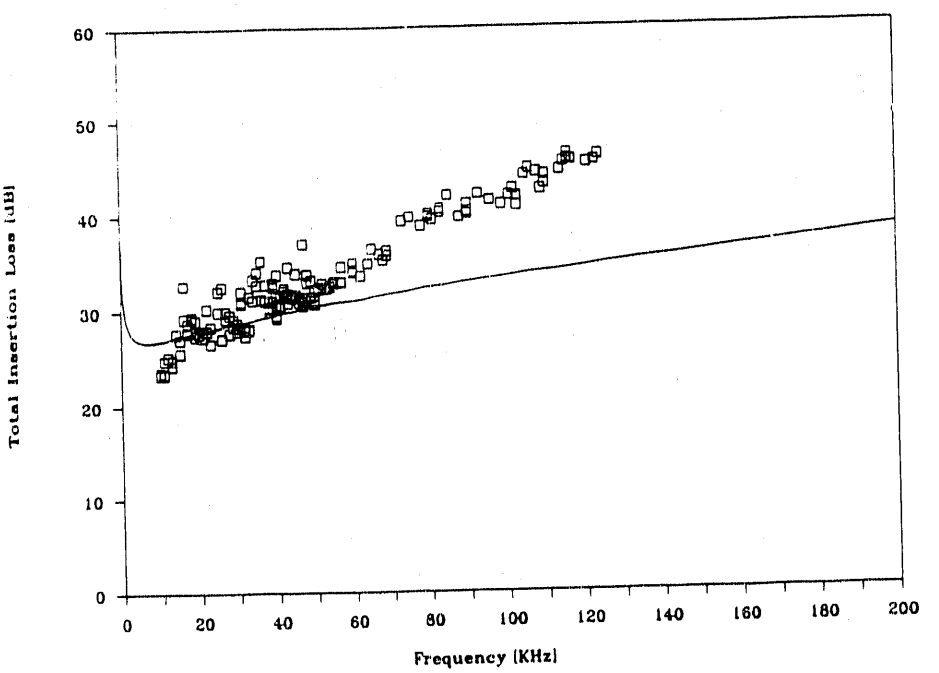

Figure 24 Normalized slow wave velocity and total insertion loss in a 1.7-mm-thick Copper Variegated Sandstone specimen.

a)

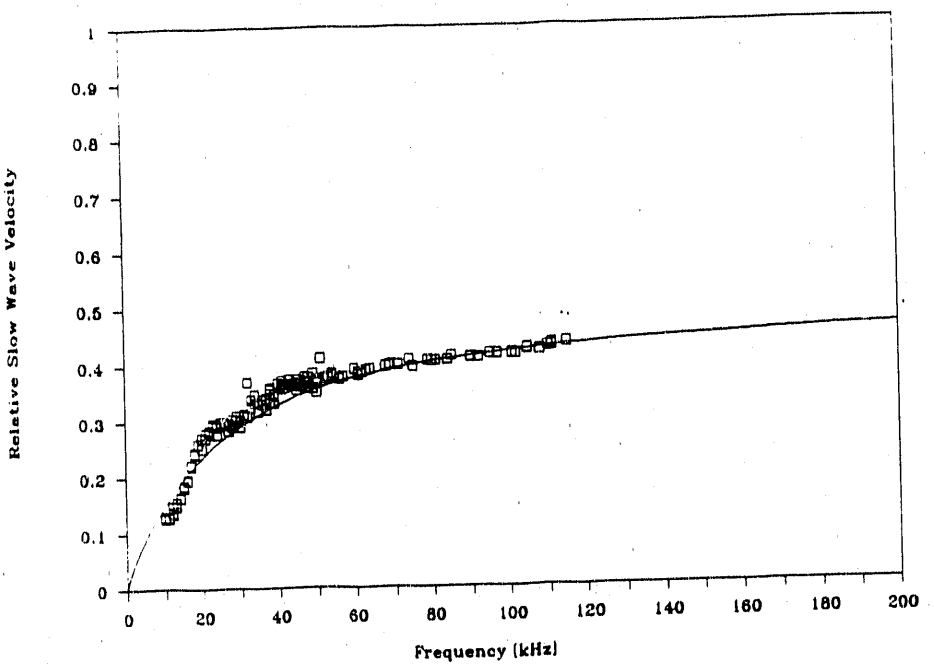

b)

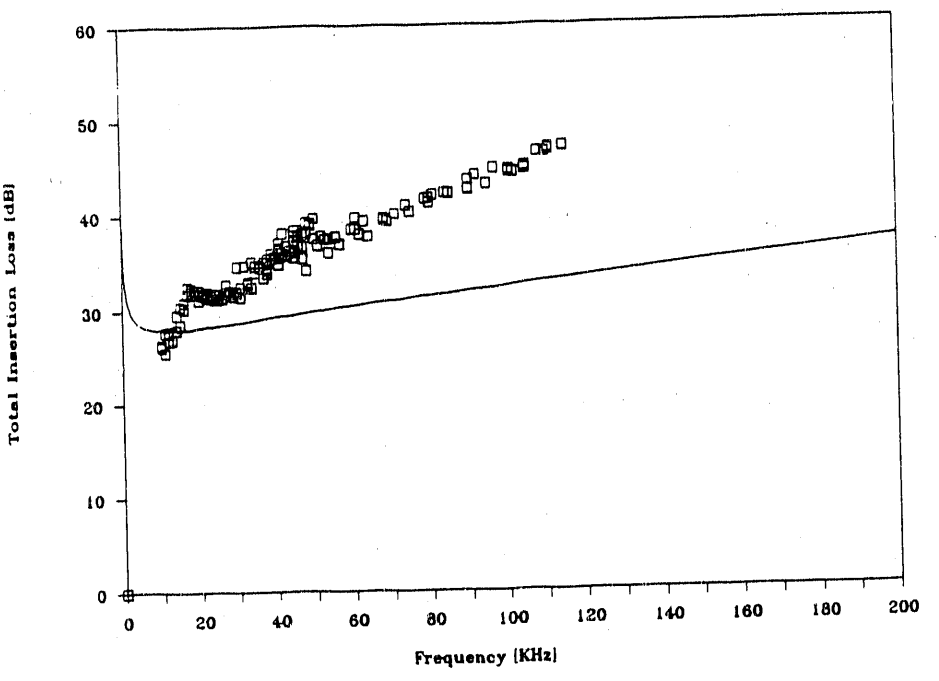

Figure 25 Normalized slow wave velocity and total insertion loss in a 1.5-mm-thick Berea Sandstone specimen.

1.2.4 DISCUSSION AND CONCLUSIONS

Transmission of airborne ultrasonic waves through thin air-filled porous plates was used to study slow wave propagation in permeable solids. We used Attenborough's theoretical model[29] to fit the experimental data and found good agreement except at high frequencies where scattering losses dominated the attenuation of the slow wave. This discrepancy has been expected since, for air saturation, there is no frequency "window" where both viscous and scattering losses are weak simultaneously. Due to the excellent sensitivity of the suggested experimental technique, low-permeability materials including natural rocks can be inspected, too. Currently, the threshold sensitivity of our system is approximately 100 mD. Further improvements can be expected from reflection-type measurements to be discussed later in more detail in the following proposal.

In the diffuse regime, i. e., at low frequencies, the velocity and the attenuation coefficient contain the same information on the permeable formation. The attenuation is linearly while the velocity is inversely proportional to the square-root of $\phi s_p^2/\kappa_o$. Since the static permeability κ_o and the pore shape factor ratio s_p always occur in the same combination through the normalized pore radius ξ, they cannot be separated by acoustical measurements. Instead, κ_o/s_p^2 was used to define a new material parameter, the so-called acoustic permeability κ_a, which can be determined from the low-frequency propagation parameters of the slow compressional wave. Comparison of the acoustic permeability κ_a and the static permeability κ_o yields valuable information on the geometry of the pore space.

Although the porosity ϕ is most easily determined by simple weight measurements on the dry and wet sample, it should be mentioned that it can be assessed by purely acoustical means, too. This is possible because both real and imaginary parts of the acoustical impedance are proportional to the square-root of

$s_p^2/\kappa_o\phi$, i. e., a different combination of the same parameters affecting the velocity and the attenuation coefficient of the slow wave. In the diffuse regime, the acoustic impedance is usually determined by reflection measurements.[27,30]

In the propagating regime, i. e., at high frequencies, only the velocity seems to be in good agreement with the theoretical predictions. Anyway, the velocity by itself is sufficient to determine the high-frequency tortuosity τ_∞ of the material while the attenuation coefficient would provide only redundant information on $\phi s_p^2/\kappa_o$ which is better determined from the low-frequency behavior. The high-frequency attenuation contains valuable additional information on the geometry of the pore space, which is related to the inhomogeneity of the pore channels. Random changes in the cross-sections of these channels cause excess attenuation by increasing the viscous drag as well as by elastic scattering. Further analytical efforts are needed to develop appropriate models for these attenuation mechanisms so that the measured data can be evaluated in terms of geometrical properties of the permeable formation. In the following proposal, we shall suggest specific techniques to develop such models.

END

DATE FILMED

8/19/92